

# Physics of Thick Polymers

Davide Marenduzzo<sup>1</sup>, Alessandro Flammini<sup>2</sup>, Antonio Trovato<sup>2</sup>, Jayanth R. Banavar<sup>3</sup> and Amos Maritan<sup>2</sup>

<sup>1</sup> *Department of Physics, Theoretical Physics, University of Oxford, 1 Keble Road, Oxford OX1 3NP, England*

<sup>2</sup> *INFM and Dipartimento di Fisica "G. Galilei", Universitdi Padova, Via Marzolo 8, 35131 Padova, Italy*

<sup>3</sup> *Department of Physics, 104 Davey Laboratory, The Pennsylvania State University, University Park, Pennsylvania 16802, USA*

## **Correspondence:**

Davide Marenduzzo, Department of Physics, Oxford University,  
1 Keble Road, Oxford OX1 3NP, United Kingdom,  
FAX: +44 1865 273947 — e-mail: d.Marenduzzo1@physics.ox.ac.uk

## **Authors' e-mail addresses:**

Davide Marenduzzo: [davide@thphys.ox.ac.uk](mailto:davide@thphys.ox.ac.uk)

Alessandro Flammini: [flammini@shannon.sissa.it](mailto:flammini@shannon.sissa.it)

Antonio Trovato: [trovato@pd.infn.it](mailto:trovato@pd.infn.it)

Jayanth R. Banavar: [jayanth@phys.psu.edu](mailto:jayanth@phys.psu.edu)

Amos Maritan: [maritan@shannon.sissa.it](mailto:maritan@shannon.sissa.it)

We present the results of analytic calculations and numerical simulations of the behaviour of a new class of chain molecules which we call thick polymers. The concept of the thickness of such a polymer, viewed as a tube, is encapsulated by a special three body interaction and impacts on the behaviour both locally and non-locally. When thick polymers undergo compaction due to an attractive self-interaction, we find a new type of phase transition between a compact phase and a swollen phase at zero temperature on increasing the thickness. In the vicinity of this transition, short tubes form space filling helices and sheets as observed in protein native state structures. Upon increasing the chain length, or the number of chains, we numerically find a crossover from secondary structure motifs to a quite distinct class of structures akin to the semi-crystalline phase of polymers or amyloid fibers in polypeptides.

## I. INTRODUCTION

Theoretical studies of polymer chains have a long history. Our focus, in this paper, is the study of a class of polymers characterized by a non-zero thickness and that can be viewed as tubes similar to garden hoses or flexible strands of spaghetti. Examples of such polymers abound and include vital biomolecules such as proteins and DNA.

Classic polymers are different from proteins on several counts. First, proteins are often very short chains made up of around a 100 or so aminoacids. Second, the aminoacid specificity plays a key role in the choice of its native state or ground state structure. One can imagine that the behavior of short chain molecules ought to be non-universal with the details mattering a great deal. To quote from Flory [1], *“Synthetic analogs of globular proteins are unknown. The capability of adopting a dense globular configuration stabilized by self-interactions and of transforming reversibly to the random coil are peculiar to the chain molecules of globular proteins alone”*.

In spite of the difficulties mentioned above, a study of the experimental data on proteins reveal an astonishing simplicity. All small globular proteins adopt, as their native conformations, structures made up of simple motifs such as helices, hairpins and sheets connected together by tight turns [2,3]. Furthermore, the total number of distinct native state folds total just a few thousand in all instead of the vastly larger number that one would expect for a conventional chain molecule of this length [4]. The structures are flexible and allow for a dizzying array of tasks that enzymes perform. One might ask where these common attributes of proteins originate from. Recent work has shown that the concept of a thick polymer might be useful for bridging the gap between polymer physics and the biomolecular phase [5–11].

Here we study a thick polymer through numerical simulations and approximate mean field theory to understand its phase behavior. Our work is somewhat limited in scope because we do not consider certain features such as twist rigidity, which are essential for understanding DNA elasticity [12,13]. It has been suggested that the effects of twist rigidity are not important for proteins [14]. Furthermore, as we shall demonstrate, the notion of thickness is sufficient to interpolate between the conventional compact polymer phase and the phase employed by nature to house protein native state structures. While non-universal behavior is expected for short chains, short chains with the right thickness exhibit very novel finite size effects with some quite robust features independent of the details. Our results are in excellent accord with experiments carried out on proteins over several decades and provide a framework for understanding the common character of proteins.

The simplest paradigm of a polymer consists of spheres tethered together to form a chain. In the continuum limit, such a model is described by the classic Edwards model [15] which captures self-avoidance by means of singular delta-function interactions. However, such a singular interaction does not admit a description of a chain of non-zero thickness and, indeed, one must renormalize it to analyze such a continuum model. Furthermore, the Edwards model is dynamically unable to preserve the knotting number of a closed chain. Indeed this result arises because the penalty for chain crossing is finite and thus crossing is not entirely forbidden. The simple model of tethered spheres is merely a starting point and it has been modified to take into account local bending energies [16] and other features that are known to play a role in experiments.

Here, we take a fresh look at the very basis of the description of a polymer chain. We suggest that a model of an isotropic sphere as the basic tethered unit leaves out a crucial feature – the inherent anisotropy associated with each unit arising from a special direction defined by the neighbouring units along the chain. Physically, we argue that this anisotropy can be captured by considering a chain made up of tethered coins or discs, which in turn leads to a tube picture of the chain. From a theoretical point of view, the model of tethered coins has the non-trivial advantage of lending itself, in a natural and singularity-free manner, to a continuum description. The singular potential is avoided because one can imagine stacking together thinner and thinner coins closer and closer together while maintaining the coin radius constant to obtain a tube of non-zero thickness [17].

One may rationalize the description of a generic polymer such as a polyethylene chain by a thick tube. Polyethylene chains have a Kuhn length around 1 nm and an approximate hard core diameter of a united atom of methylene around 0.35 nm [18]. The picture of a tube of non-zero thickness is thus a physically motivated description of such a chain and can serve as an alternative to the model of a flexible line with a  $\delta$ -function hard core self-avoidance interaction. Indeed, the key difference in the two cases is in the nature of self-avoidance.

One elegant way of describing the self-avoidance of a tube is by means of a three body potential, which enforces the constraint that a suitable length, constructed in terms of the positions of any triplet of points sitting on the axis of the tube, is greater than the tube thickness. As explained in Section III, this length associated with a triplet of points is the radius of the circle through them [19]. This length is the local radius of curvature when the three points tend to a single point on the curve, but non-local triplets play a significant role as well. The allowed configurations of a simple system of unthetered hard spheres are those in which one considers all pairs of spheres and for each pair, one ensures that the sphere centers are no closer than a sphere diameter. Such a rule ensures that the spheres are non-overlapping. The generalization of this to the chain context is to consider all triplets along the axis of the tube. Self-avoiding conformations of a flexible tube are obtained by drawing circles through each of the triplets and ensuring that none of the radii is less than the tube radius.

A tube description is useful for the understanding of proteins – the backbone of a protein, when viewed as a tube, has an intrinsic non-zero thickness in order to accommodate the steric constraints imposed by the atoms of the side chains (for a sketch, see Fig. 1). Our model is characterized by two parameters other than the length of the tube, its thickness  $R_0$  and the range of the attractive potential  $R_1$ . When these two lengths are comparable, we find that the ground state configurations of a short tube closely resemble the secondary motifs of folded proteins. We will demonstrate that these configurations change to amyloid-like structures upon increasing the tube length. We will present detailed studies of the phase diagram and will discuss similarities and differences with those obtained with previously studied polymer models. Through an extensive statistical analysis of triplet radii in known ground states of proteins, we found that the average thickness of a protein is 0.27 nm [8]. Consequently, the typical values of  $R_0$  and of  $R_1$  are matched in native structures of proteins, where  $R_1 \simeq 0.55$  nm, when intra-chain hydrogen bonding is considered.

There are several new features, both at local and non-local levels, that are characteristic of a tube. First, there is a constraint on the local radius of curvature which forbids the radius from being smaller than the tube thickness. This constraint is different from the bending rigidity potential energy [16] which is usually taken to be of the form  $\kappa(1 - \cos(\theta))$  where  $\kappa$  is a positive coupling, and  $\theta$  the angle between successive links – as the temperature is lowered the chain becomes straighter. In contrast, the local radius constraint in a tube is a rigid constraint which is independent of temperature. In addition, the tube imposes a non-local constraint which, physically, reflects the fact that different segments of a tube cannot approach each other closer than a threshold distance governed by the tube thickness. This is captured by imposing that no three-body radius (of any non-local triplets) can be smaller than the tube thickness. In order to best avail of the attractive interactions between different parts of a tube, the relative orientation of neighbouring segments becomes important reflecting the inherent anisotropy associated with a tube [20,21].

These new features lead to a phase diagram in which one can distinguish between three classes of tube thickness. In the thin tube regime, one obtains two distinct phase transitions on lowering the temperature from the swollen phase. First one enters an isotropic collapsed phase which is supplanted by an oriented nematic-like phase after the second phase transition. For intermediate thickness, there is only one phase transition to an oriented, compact phase while, for larger tube sizes, one simply obtains the swollen phase.

Our studies of short tubes in the intermediate thickness regime show several unusual characteristics. First, the number of ground state structures is much smaller than the corresponding number for chains of spheres: the energy landscape is vastly simpler. Second, the resulting structures are marginally compact (the effects of attractive self-interactions have just set in) and, because of their proximity to a phase transition, are sensitive to the right types of perturbations. Strikingly, we find that the resulting structures are predominantly space-filling helices (with a specific pitch to radius ratio) and nearly planar zig-zag hairpin and sheets. These structures are found to be quantitatively akin to the building blocks of protein structures. Our results indicate the presence of a previously unstudied phase of matter, associated with short tubes of intermediate thickness, which has many attendant advantages exploited by nature in housing biomolecular structures. Our results show that the tube picture provides a unified framework for understanding the common character of small globular proteins. Upon increasing the length of the polymer, or the number of polymer chains, we observe, in computer simulations, a crossover to semi-crystalline structures with different portions of the backbone chain lying parallel to one another. Significantly, this low temperature anisotropic phase of tubes provides a simple rationalization for the formation of amyloid in misfolded proteins (leading to deadly diseases, including Alzheimer’s and the Mad Cow disease [30]) and the formation of semicrystalline polymer.

There are some remarkable differences between the behavior of our model and that of a stiff chain as embodied by the semiflexible chain model [31–33]. The phase diagrams of a self-interacting tube and a semiflexible chain both display three phases: a swollen phase, an isotropic collapsed phase, and an anisotropic globular phase (semi-crystalline phase). However, the phase boundaries look rather different. In particular, there is a zero-temperature first order phase transition in the thick polymer case which is observed on increasing the thickness, which has no counterpart in the stiff polymer phase diagram. Moreover, the thickness acts as a constraint on viable configurations, while the bending rigidity acts as an energetic penalty. Technically, this leads to the swollen phases being somewhat different in that in the continuum limit the typical tube centerlines are smoother than the semiflexible chain backbones. Also short tubes of intermediate thickness yield helices and almost planar zig-zag conformations, a feature absent in the semi-flexible chain model.

Our paper is organized as follows. Section II presents a brief review of the Edwards model. Section III presents the tube picture of a polymer chain and its advantages. Section IV deals with studies of the ground states of short chains subject to self-attraction and underscores the qualitative differences between chains of spheres (with or without bending energies) and short tubes. We review work which shows that the latter describes a novel phase used by nature to house biomolecular structures.

Section V presents an attack on deducing the phase diagram of tubes using several complementary techniques. Some of the technical details are relegated to an appendix. We conclude with a brief summary in Section VI.

## II. EDWARDS MODEL OF A POLYMER CHAIN

Field theory models have proved to be useful for carrying out analytic calculations of the scaling behavior of polymers. The standard model is that due to Edwards – the polymer is described by a continuous curve,  $\vec{r}(s)$ , with an effective energy given by

$$H(\{\vec{r}\}) = \frac{1}{2} \int_0^L \dot{\vec{r}}(s)^2 ds + \frac{v_2}{6} \int_0^L \int_0^L \delta(\vec{r}(s) - \vec{r}(s')) ds ds' + \frac{v_3}{90} \int_0^L \int_0^L \int_0^L \delta(\vec{r}(s) - \vec{r}(s')) \delta(\vec{r}(s) - \vec{r}(s'')) ds ds' ds'' + \dots \quad (1)$$

The first term in the above equation takes into account the chain entropy and arises from the central limit theorem. It is readily derived for a non-interacting chain of beads (the location of the  $i$ -th bead is denoted by  $\vec{r}_i$ ) tethered together by a potential  $u(r_{j,j+1})$ , with  $r_{m,n} = \|\vec{r}_n - \vec{r}_m\|$ , acting between adjacent beads and keeping them at a typical mean square distance  $b^2$ . Using the central limit theorem, one finds that the probability of finding the first bead at  $\vec{r}_1$  and the  $k$ -th bead at  $\vec{r}_k$  is well approximated by

$$P(\vec{r}_1, \vec{r}_k) \propto \exp\left\{-\frac{d}{2b^2k}(\vec{r}_1 - \vec{r}_k)^2\right\} \quad (2)$$

for large  $k$ . Consider now a ‘coarse-grained’ chain made up of  $n$  pieces of such  $k$ -step chains. Let the  $i$ -th piece start at the position  $\vec{r}_{(i-1)k}$  and end at  $\vec{r}_{ik}$  for each  $i = 1, 2, \dots, n$ . It then follows that the probability of obtaining this configuration of the chain is given by

$$P(\vec{r}_0, \vec{r}_1, \dots, \vec{r}_n) \propto \exp\left\{-\frac{d}{2b^2k} \sum_{i=1}^n (\vec{r}_{(i-1)k} - \vec{r}_{ik})^2\right\} \quad (3)$$

In the continuum limit, one defines  $\epsilon = kb^2/d$  and the total ‘length’ of the ‘coarse grained’ chain,  $L = n\epsilon$ , is kept fixed while  $n \rightarrow \infty$  (this implies that  $b \rightarrow 0$ ). In this limit, the previous equation leads to the Hamiltonian (Eq. (1)), in the non-interacting case ( $v_i = 0, i = 2, 3, \dots$ ), because

$$\lim_{\epsilon \rightarrow 0} \sum_{i=1}^n (\vec{r}(t_{i-1}) - \vec{r}(t_i))^2 / \epsilon = \int_0^L \dot{\vec{r}}(s)^2 ds \quad (4)$$

where  $\vec{r}_{ik} = \vec{r}(t_i)$ .

In the self interacting case, one again starts from a string of beads as before, where the total energy is given by,

$$H_{chain} = \sum_j u(r_{j,j+1}) + \sum_{m < n} V(r_{m,n}) \quad (5)$$

where  $V(r)$  is a two-body interaction between pairs of beads at a distance  $r$ . The shape of  $V(r)$  is typically similar to the classic 6-12 Lennard-Jones potential with attraction at intermediate length scales and repulsion when two beads get too close to each other. A link between Eq. (5) and the continuum model Eq. (1) can be established through the virial expansion.

The  $v_m$ 's in eq.(1) represent effective  $m$ -body interactions for the continuum chain,  $\vec{r}(s)$ , and they depend on the temperature,  $T$ . In order to get a swollen phase at high temperatures and a compact phase at low temperatures, at high (low)  $T$ ,  $v_2 > 0$  ( $v_2 < 0$ ) whereas  $v_3 > 0$ . The three-body term is strictly necessary only in the low temperature region in order to stabilize the system. The model defined by eq.(1) is widely used in the literature and it has been shown to have a precise meaning in perturbation theory using renormalization group techniques (see [34–36] and the original references therein) [37]. However, it has been suggested by Barrett and Domb [40] that *the renormalization group has not provided a satisfactory description of a polymer in the poor-solvent (weak coupling) regime, perturbation methods are hopelessly incapable of describing the good solvent (strong-coupling) regime, there is no entirely satisfactory description of the crossover from poor solvent to good solvent conditions, and the limits in which excluded-volume chains exhibit universality are not fully understood.*

One may understand heuristically why the continuum version of eq.(5) can only give rise to interaction terms which are singular (the  $\delta$ -function potentials in eq.(1)). Let us make the physical assumption that the potential  $V(r)$  in eq.(5) has a

repulsive part which becomes larger as  $r$  decreases. In order to take the continuum limit, the bead density along the chain must increase, because the tethering  $u$  potential constrains successive beads to lie closer to each other as  $b \rightarrow 0$ . As  $b$  decreases, the number of bead-pairs within the repulsive region of the  $V$  potential increases and, in the continuum limit, the chain would have an infinite energy and an infinite rigidity. As  $b \rightarrow 0$ , this unphysical consequence can be avoided by simultaneously shrinking the size of the repulsive region of the interaction potential  $V$  in eq.(5) leading to singular  $\delta$ -function potentials in the continuum limit as in eq.(1).

Furthermore, there does not exist, to our knowledge, a continuum formulation of closed polymers which allows one to carry out studies within a given knot class, i.e. with a fixed number of knots. Indeed, a drawback of any formulation using two-body potentials, such as eq. (1)), is that the self-intersection of the chain is allowed albeit with some energetic penalty and thus one can change, at will, the topology of the polymer. This is not what happens in realistic situations. Furthermore, there are interesting physical problems pertaining to the estimation of entropic exponents and weights of polymer configurations within a given topology [41,42]. While such calculations can be carried out numerically, at present, there is no simple analytic formulation of this problem.

A simple discrete model of spheres tethered together in a chain would lead, in the continuum limit, to the Edwards model. As the distance between successive spheres shrinks, so must the radius of the spheres and in the limit one obtains a string of infinitesimal thickness. So how would one describe mathematically a string of non-zero thickness analogous to a tube or a garden hose or a spaghetti? Is there a way to avoid a singular interaction potential? More important, is the physics of thick strings qualitatively different from that predicted by the Edwards model? Our focus, in this paper, is on answering these questions.

### III. TUBE PICTURE OF A POLYMER CHAIN

In this section, we provide a brief description of how one might describe a tube of non-zero thickness. Let us consider the general case when the interacting particles (monomers) are restricted to lie in  $D$ -dimensional manifolds such as a string ( $D = 1$ ) or a surface ( $D = 2$ ) embedded in  $d$ -dimensional space. Examples of such systems include strings and random surfaces and are widely studied in many branches of science [43,44]. The interaction (tethering) potential leading to the system being restricted in the form of a manifold or bending rigidity terms are not our concern here – there are many satisfactory ways to construct such a potential for strings and surfaces. Our focus is on the self-interaction not captured by the tethering potential. This self-interaction between the monomers are meant to be effective interactions resulting from the elimination of the finer degrees of freedom. We will argue that the basic interacting unit must have at least  $D+2$  monomers in order to define a meaningful characteristic length associated with this interaction. Such a basic many-body interacting unit is necessary for a continuum approach to these classes of problems. Note that for unconstrained particles,  $D = 0$  and pair-wise interactions suffice.

Consider a  $D = 1$  system of a string in  $d = 3$ . In order to account for steric interactions, that prevent the string from intersecting with itself, one might postulate a pairwise potential which becomes large when two of the constituent particles are near each other. However, given two nearby particles, it is impossible to distinguish whether they are from distinct parts of the string or whether they are close by simply because of the string connectedness. As one approaches the continuum limit by increasing the density of particles along the string and shrinking the distance between them, the energy contribution from the latter category of pairs, which are close to each other essentially because of the tethering potential, vastly exceeds the contribution from particles that are genuinely responsible for a self-intersection. There is no inherent small-distance cutoff in the theory and regularization procedures are needed that re-introduce such a length scale in order to avoid infinities.

The requirements for a well-founded theory are that one ought to be able to take a continuum limit on increasing the density of particles, that self-interactions be properly taken into account and that there be a characteristic microscopic length other than the spacing between neighboring particles along the string. As explained above, a pairwise potential is not equal to the task. Let us consider a three-body potential characterizing the interaction between three particles, which lie on the corners of a triangle. Let the sides of the triangle have magnitudes  $r_1$ ,  $r_2$  and  $r_3$ . In order to specify a triangle uniquely, one needs three attributes. The potential of interaction can therefore depend on three independent length scales, which are invariant under translation, rotation and permutation of the three particles. One may choose these length scales to be the perimeter,  $P$ , of the triangle, the ratio of the area,  $A$ , of the triangle to its perimeter,  $P$ , and finally  $r_1 r_2 r_3 / A$ . The first two lengths do not cure the problems alluded to before – they both vanish when the particles approach each other either from the same region or different regions of the string. The third length scale is proportional to  $R$ , the radius of a circle drawn through the three particles and has proved to be valuable for the study of knots [5].

If one considers the minimum over all triplets of this quantity, that is just the ‘thickness’ [19] of the continuum curve we are considering – the thick curve may be thought of as a tube or a thick polymer. The key result is that the description of the effective self-interactions of a string, which satisfies all the requirements of a well-founded theory will involve a three body

potential,  $V_3(R)$ , among all triplets of particles in the string. In this case, the continuum limit can be taken safely, self-avoidance is respected and a cut-off scale naturally arises through the functional form of  $V_3$ , in this case a hard-core form.

One may illustrate the difference between the approach to the continuum limit in the chain of spheres model and the tube model in the following manner. Consider first a self-avoiding chain made up of spheres tethered together with the distance between successive spheres equal to the bond length  $b$ . Let  $R_{hc}$  represent the hard core radius of the sphere. Physically,  $b$  is expected to be of the order of  $2R_{hc}$ . For a chain of length  $N$ , one may, from general considerations, write the radius of gyration as  $R_g(N, b, R_{hc}) = R_{hc} F_s(N/R_{hc}, b/R_{hc})$ . In order to take the continuum limit, one must let  $b$  approach 0. But this automatically constrains  $R_{hc}$  to go to zero as well, while maintaining the ratio of  $b/R_{hc}$  at some suitable non-zero value. This immediately poses a problem because, in order for one to obtain the well-known result that  $R_g$  scales as  $N^\nu$ , there is no other non-zero length scale in the problem. The cure for this, of course, is to use renormalization procedures by introducing an artificial cutoff followed by a demonstration that the answers do not depend on the cut-off.

This problem is nicely avoided in a tube description within which  $R_g(N, b, R_0) = R_0 F_t(N/R_0, b/R_0)$ , where  $R_0$  is the tube thickness. The only constraint on  $b$  now is that it is less than or at most comparable to  $R_0$ . Thus, the continuum limit can be safely taken by letting  $b$  go to 0 and obtaining  $R_g = R_0 F_t(N/R_0, 0) \sim R_0^{1-\nu} N^\nu$ . In other words, the nonzero thickness (as embodied in a suitable three body potential) of a tube provides a suitable cut-off length scale and avoids the singularity implicit in the conventional Edwards model and the absolute need for the use of renormalization techniques [39], allowing for the first time analytic studies of polymers with fixed knotting numbers. In the continuum limit, the many-body potential replaces the pairwise self-interaction potential and ought not to be thought of as a higher order correction [45].

Nevertheless, for discrete models of a thick tube, two-body interactions do not suffer from the problem described above and can coexist with three-body terms which model the non-zero thickness of the curve approximately. Consider the Hamiltonian for a string of the form

$$H_{chain} = \sum_i u(r_{i,i+1}) + \sum_{i<j} V_2(r_{i,j}) + \sum_{i<j<k} V_3(r_{i,j,k}), \quad (6)$$

where, as before  $u$  is a generic tethering potential,  $V_2$  is a pairwise potential and  $V_3$  is a three-body potential. In most of our simulations, we have chosen  $u$  to constrain  $r_{i,i+1}$  to be constant. The pair potential is taken to be

$$V_2(r_{i,j}) = \begin{cases} \infty & \text{if } r_{i,j} < 2R_{h.c.} \\ -1 & \text{if } 2R_{h.c.} < r_{i,j} < R_1 \\ 0 & \text{if } R_1 < r_{i,j} \end{cases} \quad (7)$$

where  $R_1$ , the range of the attractive interaction is taken to be 1.6 units (measured in units of the bond length or the fixed distance between successive beads, which is chosen to be 1) in our simulations and  $R_{h.c.}$  is the hard core radius, which we take to be 0.55 in our calculations. These values have been selected in order to mimic values typical of a protein backbone (see Introduction). We verified that small changes in the attraction range do not change the results shown here appreciably (see Fig. 4). A Lennard-Jones potential for the two-body interaction energy, with an equilibrium distance slightly larger than the neighbouring site distance, is also expected to give qualitatively similar results, provided the potential is truncated in order to eliminate the unphysical effects of a long range tail.

The three body potential [19,47],  $V_3$ , disallows conformations for which  $R_0 > \min_{i \neq j \neq k} r_{i,j,k}$ , where  $r_{i,j,k}$  is the radius of the circle going through the centers of the beads  $i$ ,  $j$  and  $k$  (Fig. 2). This three body constraint leads, in the continuum limit, to a tube of radius  $R_0$ , whose axis is given by the string defined by  $\vec{r}_i$  (see Fig. 2). This can be simply proved by noting that the quantity  $\min_{i \neq j \neq k} r_{i,j,k}$  is the thickness of the maximally inflated tube with centerline  $\{\vec{r}_i\}_{i=1, \dots, N}$  [19]. If the maximally inflated tube has a thickness greater than  $R_0$ , then this means that the discrete curve under analysis is a viable centerline for a tube of thickness  $R_0$ . For the discrete case, the three-body constraint is not as severe as in the continuum limit – we will show that discreteness can play a vital role in producing planar structures for short tubes subject to self-attraction.

In the remaining sections, we will demonstrate, using various complementary techniques, that a rich variety of new phases is obtained for a tube subject to self-attraction, which allow a bridging of conventional polymer phases to a novel phase used by nature for housing biomolecular structures.

#### IV. GROUND STATES OF SHORT CHAINS

Our focus, in this section, is to discuss the ground state structures of short chains subject to self-attraction. Strikingly, marginally compact tube structures have helical, hairpin and sheet configurations which are the building blocks of protein

native state structures. We will consider the structures adopted by a tube and by a chain of spheres in order to understand the common features of both classes and underscore the qualitatively new features introduced on incorporating the intrinsic local anisotropy of a chain. We will also assess the nature of the structures adopted by a stiff chain, or equivalently a semiflexible polymer, subject to compaction. This analysis demonstrates that, at least, within the parameter range we have explored, there is less secondary structure content in short semiflexible chains in clear contrast to the marginally compact phase obtained for a tube.

Hard spheres are the simplest basic entities for modelling matter. In spite of their simplicity, hard spheres exhibit an entropy-driven phase transition between a fluid phase at low packing fractions and a crystalline phase at high packing fractions. The favored crystalline structure is that of a face-centered-cubic crystal which allows for the most efficient packing. In two dimensions, hard disks would prefer to pack most efficiently in a triangular lattice. Let us now consider a chain molecule made up of tethered hard spheres (in three dimensions) or tethered disks (in two dimensions). For simplicity, let us restrict ourselves to the simplest case in which the tethering constraints for compact conformations are not frustrating and lead to the same ground state as in the untethered case. This greatly simplifies the analysis of the ground state conformations of compact chains because one can carry out the analysis for unconstrained, untethered objects first and imagine placing the tethers through the resulting ground state structure(s).

The systems that we will study (without and with the three body tube constraint, and with the stiffness term) are all subject to the same attractive potential energy of interaction. They consist of a chain of spheres subject to a pair-wise attractive potential – a pair of spheres, at  $\vec{r}_i$  and  $\vec{r}_j$ , have an interaction given by eq. 7. There is an additional constraint for the tube case which forbids any of the three-body radii associated with the spheres of the chain from being smaller than the tube thickness  $R_0$  (potential  $V_3$  in eq. (6)). Finally, for a chain of spheres with a non-zero stiffness [31,32], we complement the two body potential in Eq. 7 with a bending-rigidity term of the form:

$$H_b = -\kappa \sum_i \vec{r}_{i,i+1} \cdot \vec{r}_{i+1,i+2}, \quad (8)$$

with  $\kappa$  a constant, the chain stiffness, and with  $\vec{r}_{i,i+1} = \vec{r}_{i+1} - \vec{r}_i$ . We will point out similarities and differences between these three cases.

## A. Geometry of chains of spheres

We begin with an analysis of the chain *without* the three-body constraint. In this case,  $R_{h.c.}$ , the hard-core radius is held fixed at a value of 0.5 and we will consider the nature of the ground state structures on varying  $R_1$ , the range of the attractive interaction. Recall that while our focus is on chains of spheres (or disks), the tethering constraint does not play a role for the selection of compact conformations. The role of the tethering constraint here is simply to enhance the degeneracy of the ground state. This is because there is an exponential (as a function of the length) number of ways in which one might accommodate the tether through a packed configuration of beads. A well-known example is provided by Hamiltonian walks, which are the ensemble of configurations of chains filling a finite sized square lattice [48]. For simplicity, here we will consider just the degeneracy of the underlying conformation of spheres without taking into account this extra degeneracy.

### *Two-dimensional case*

In  $d = 2$  it is well known that there is a unique way of packing hard disks so that the packing is most efficient. This optimal packing is performed by placing the centers of the disks on a triangular lattice, whose lattice parameter equals the disk diameter. Each disk is then surrounded by six nearest neighbors. This is indeed the ground state structure of tethered disks when  $R_1 = 2R_{h.c.}$ . Let us first discuss the nature of the ground state structures for arbitrary values of the attraction range  $R_1$  in the thermodynamic limit. Finite size effects are less relevant here and will be considered carefully for the tube and semi-flexible chains considered later on in this Section, and, for the two-dimensional case, will be briefly discussed at the end of this sub-section.

When the number of disks or spheres becomes large, one expects the ground state to be a translationally invariant lattice. When  $R_1 < 2R_{h.c.}$ , the disks are unable to avail of the attractive interaction and one obtains a swollen phase – all conformations of the chain which do not violate the hard disk constraint are equally likely. We now turn to an analysis of the compact conformations that one obtains when  $R_1 > 2R_{h.c.}$ .

Figure 3 shows a sketch of the winning lattice structures as a function of  $R_1$  in the compact phase (the lattice considered are all Bravais two-dimensional lattices, defined by the angle between two unit vectors). The ground state is non-degenerate at  $R_1 = 2R_{h.c} = 1$ , but on increasing  $R_1$ , the degeneracy goes up (see shaded region in the figure) until a value of  $R_1 = \sqrt{2}$ , when the ground state is non-degenerate and corresponds to a square lattice with lattice parameter equal to 1. In this structure,

both the nearest neighbors and next-nearest-neighbors are able to avail of the attractive potential.

Strikingly, this pattern of non-degenerate ground states for selected values of  $R_1$  followed by segments characterized by huge degeneracies repeats as  $R_1$  increases. Of course, in the limiting case of very large  $R_1$ , one recovers the swollen phase and each disk feels an attraction with every other disk. We have verified, with Monte-Carlo simulations, that for small systems of the order of, say, 25 disks, finite size effects dominate but one can be reasonably sure that non-translationally invariant structures do not win over the Bravais lattices that have been considered in our exact calculations reported in Figure 3.

### *Three-dimensional case*

We have also studied the three dimensional case of a chain made of tethered hard spheres. As before, when  $R_1 < 2R_{h.c.}$ , one obtains a swollen phase consisting of self-avoiding conformations of the chain. When  $R_1 = 2R_{h.c.}$ , one not only obtains the fcc lattice with lattice parameter of 1 as the ground state but there is an essentially infinite degeneracy in the thermodynamic limit of random hexagonal close packed stackings. This is well known in the context of hard sphere colloids [49,50]. Of all these degenerate structures, the fcc structure is the only Bravais lattice. For the situation with  $R_1 > 2R_{h.c.}$ , we have considered all three dimensional Bravais lattices and identified those that correspond to the minima of the potential energy. As before, there are huge degeneracies in the ground state conformations and discontinuous jumps in the ground state energies as the range of the interaction is changed. It is interesting to note that one of the ground states corresponds to stacked triangular lattices, previously observed by Zhou et al. [51]. The unit cell of this three dimensional lattice has two triangular faces and the other faces are squares.

There are several common features in our results:

- 1) On increasing the range of attraction, one can identify an edge of compactness at which the attractive interaction just kicks in (when  $R_1 = 2R_{h.c} = 1$ ) and the swollen phase gets replaced by a triangular lattice in two dimensions and a fcc or hcp lattice in three dimensions.
- 2) In general, the arrangement of the spheres comprising the chain is symmetric. A given sphere is surrounded isotropically by other spheres to attain the best packing.
- 3) One obtains a unique ground state for only certain very special values of the range of the attractive interaction. In general, the degeneracy increases as one moves to the right of a plateau or as the range of the attraction increases in magnitude.
- 4) There are discontinuous jumps in the ground state energy on changing the range of the attractive interaction.
- 5) The ground state structures in different plateaus (as in Figure 2 for the two dimensional case) are, in general, not the same.

In the next sub-section, we will turn to an analogous study of spheres tethered together as before but this time with a three body constraint that captures the tube thickness. Note that the interacting objects have an effective anisotropy. Furthermore, there is an additional length scale – the thickness of the tube. We will consider ground state conformations of such a tube on varying  $X$ , defined as the dimensionless ratio of the tube thickness to the range of the attractive interaction. We will find many features that are reminiscent of our results in this section: there are discontinuous jumps in the energy on increasing  $X$  with a non-degenerate ground state at the end of each plateau. The key difference is that because of the inherent anisotropy of a tube, a careful relative positioning and orientation of nearby tube segments are needed in order to avail of the attractive interaction. This leads to huge reductions in the degeneracy of tube conformations. Furthermore, for short tubes, at the edge of compactness, one obtains helix, hairpin and sheet conformations which are the building blocks of protein structures.

The above picture ought to be robust on replacing the discontinuous square well potential for the two-body interaction energy with a continuous Lennard-Jones potential. The main difference would be the absence of discontinuous jumps in the energy, but a plateau could still be defined by monitoring the switching of the underlying ground state conformations, as in the case of short stiff chains in the presence of a continuous bending rigidity potential (see sub-section C).

## **B. Geometry of short tubes**

In this sub-section, we will present a brief review of the results of our simulations of short tubes [8,9]. The potential energy is as before but with a three body constraint that does not allow any triplet radius to be smaller than the tube thickness  $R_0$ . Again, we hold the successive tethered spheres at a mutual distance of 1 unit, the hard core radius of the sphere  $R_{h.c.}$  is held fixed at 0.55 and the range of the attractive interaction is maintained at 1.6 units. We now vary the tube thickness  $R_0$  (and hence the dimensionless ratio  $X$ ) and seek to determine the conformation(s) for which the potential energy is as low as possible. Thus we seek the tube analogs of the Bravais lattice structures that we discussed in the previous sub-section.

As before, when  $X$  is very large compared to 1, the tube is so fat that it is unable to benefit from the attractive interactions. The constraints of the three body interaction dominate (the pairwise interaction plays no role) and one then obtains a swollen phase – all self-avoiding conformations of the tube are equally likely and the vast majority of them is not effective in filling the space in the core of the structure. Note that globular proteins fold in order to squeeze out water from the core of the folded



state, which houses the hydrophobic amino acids. At the other extreme, for a tube with a very small  $X$  compared to 1 (very thin tube), one obtains many conformations, leading to an energy landscape studded with numerous multiple minima. We thus expect a transition to occur for intermediate value of  $X$ , when the thickness is comparable to the attraction range (see Figure 4). We shall denote the resulting conformations near this transition as being marginally compact structures because they lie at the edge of the compact phase – a small increase in the tube thickness is sufficient to change these into swollen conformations unable to avail of the attractive potential. Protein structures live in the marginally compact phase because the side chains of the amino acids, on the one hand, determine the tube thickness (note that steric overlaps of the side chains has to be respected) and, on the other, control the range of the interactions (the atoms of nearby sidechains interact through a screened, attractive short range interaction). This self-tuning is a marvelous attribute of proteins.

Our goal is to study the ground state conformations on varying the tube thickness. For a short tube, made up of  $N$  balls, subject to pair-wise attractive interactions, let us denote by  $N_c(N, R_0)$  the maximum number of contacts (each with an energy of  $-1$  – Eq. (7)) that can be made without violating both the hard-core and the three body constraints. Quite generally, one would expect that, for a fixed  $N$ ,  $N_c$  is a decreasing function of  $R_0$  and that the decrease occurs in discrete steps corresponding to the inability to form the same number of contacts as before. Physically, of course, for a given contact energy (or equivalently the number of contacts), one would choose the largest possible thickness in order to provide as much internal wiggle room (for the amino acid side chains, in the case of a protein) within the tube as possible.

We have carried out Monte-Carlo simulations by using the standard simulated annealing algorithm in order to find the ground state of the thick polymer. This basically entails starting from a swollen disordered configuration at a high temperature,  $T$ , and monitoring the collapse on gradually lowering the  $T$ . On repeating this procedure many times, one hopes to find a good approximation to the ground state conformation of the tube. It is well known that this procedure may lead to the system being ‘trapped’ in metastable minima. We have attempted to avoid this in two ways: first, by repeating the simulation many times, changing the algorithm parameters (such as the amplitude of the dynamical moves), and second, by comparing the annealing performance with that of a recently proposed algorithm [52] for finding the density of states of a system reliably. The results presented here are independent of the algorithm used to obtain them.

We have carried out simulations for several values of  $N$  and present the scenario for  $N = 14$ , which is representative of values of  $N$  between 6 and 20. A schematic “phase diagram” is shown in Figure 4, while Figure 5 is a plot of  $N_c$  (or equivalently the negative of the ground state energy) as a function of the tube thickness. For small  $R_0$  one gets a highly degenerate phase with  $N_c$  saturated at a value of 45 for  $N = 14$  – the conformations that the tube adopts depend rather strongly on the details of the pair-wise potential. For  $R_0$  between  $\sim 0.75$  and 0.8, there is an energy plateau in which the degeneracy is greatly reduced and helices are the ground states. Furthermore, for the tube with the largest thickness in this plateau, one obtains a specific helix as the unique ground state (see upper conformation in “Marginally compact phase” of Fig. 4 and Fig. 6 (A2)). For  $R_0$  between 0.8 and 0.98, several classes of conformations including saddles (which are planar hairpin conformations distorted into three dimensional structures) (see Fig. 6 (C2)), generalized helices (in which the distance between successive balls along the helical axis is not constant but is periodic) (see Fig. 6 (A3)), helices made up of strands (see Fig. 6 (B2)) and other more disordered conformations compete.

At the end of each plateau in Figure 5 (there are as many as three major plateaus in this range of tube thickness, and each plateau comprises several distinct sub-steps or smaller plateaus), we find an ordered unique ground state (see some examples in Fig. 6, second row). (The robustness of our results is underscored by the fact that helices and sheet-like conformations emerge as the conformations of choice at the end of some of the major plateaus for other parametrizations of the potential energy of interaction as well [8].) One may show that helices are excluded from being the ground states, when the tube thickness exceeds  $R_0^{max, hel} \sim (\sqrt{1 + R_1^2})/2 \sim 0.943$  which is obtained when two parallel straight lines (successive turns of the helix treated as circles with infinite radius) face each other at the bond length  $R_1$ .

For  $R_0 > 0.98$ , the ground state structures become more and more planar, first locally and then globally. For large  $N$ , the winning planar structures entail the combinations of strands into a sheet structure. (We find that sheet structures persist for  $N$  as large as 24, whereas the persistence length for helices is expected to be somewhat smaller.) For two zig-zag antiparallel strands facing each other, one can show analytically that the maximum thickness is obtained (leaving aside the edge effect of how the strands are connected together in a hairpin) when one has a space-filling conformation [53], and furthermore when the local and the smallest non-local radii of curvature have the same value. Indeed, this condition leads to the following relationship between the tube thickness  $R_0$  and the interaction range,  $R_1$ , as defined in eq. (7)

$$R_1^2 + 2 + \frac{R_1}{R_0} - 4R_0^2 = 0, \quad (9)$$

which yields a value of  $R_0 \sim 1.2124$ , when  $R_1 = 1.6$ . Eq. 9 can be obtained by means of simple geometrical considerations – one wishes to maximize the function  $\min_{i,j,k} R_{ijk}$  with respect to  $\theta$ , the angle between two successive links in the zigzags, and  $x$ , the distance between the two strands. One can readily show that the maximum thickness is obtained for a planar configuration.

In Fig. 7, the sum of the three angles  $\theta$  and  $\phi_{1,2}$  is  $2\pi$ . When the configuration is bent along the contact axis ( $AB$  in Fig. 7) the angle between two successive links  $\theta$  will be smaller and as a consequence the local thickness (which is  $1/(2 \cos(\theta/2))$ ) will be smaller. For a rotation of the left zig-zag strand around the axis  $AC$ , on the other hand, either  $\phi_1$  or  $\phi_2$  will become smaller and again the thickness will decrease.

The swollen phase, which occurs for even larger values of tube thickness, has two energy plateaus. The first of these plateaus has just one contact and comprises all swollen conformations whose two ends make a contact (i.e. ring-like configurations) – the thickest tube which is able to make 1 contact has a unique ground state of a closed polygon with  $N$  edges of unit length and 1 of length  $R_1$ . Likewise, the plateau of 0 contacts has the limiting thickness situation of a straight, infinitely fat tube. Indeed, starting from the zig-zag conformation, the unique conformations corresponding to the largest possible thickness compatible with a given energy (or number of contacts) all share the intriguing property that the local and the smallest non-local radius are exactly equal (It is interesting to note that the optimal helix of Fig. 6 (A1) has a ratio of the smallest non-local to the local radius of around 0.97 which is very close to the corresponding value for  $\alpha$  helices occurring in proteins [6,7]).

Helices and sheets are, of course, the well-known building blocks of protein structures [2,3] (see Fig. 6 (A1) and (D1) for two examples). In addition to the prediction of these motifs in our calculations, it is interesting to note that some of the other marginally compact conformations bear a qualitative resemblance to secondary folds in biopolymers. Helices analogous to Figure 6 (A3) with an irregular contact map occur, e.g., in the HMG protein NHP6a [54] with pdb code 1CG7. Fig.6 (C1) shows the “kissing hairpins” [55] of RNA (pdb code 1KIS), each of which is a distorted and twisted hairpin structure while Fig. 6 (C2) is a saddle conformation, which is a hairpin distorted into a three-dimensional structure. Figure 6 (B1) shows a helix of strands found experimentally in Zinc metalloprotease [56] (pdb code: 1KAP), whereas Figure 6 (B2) is the corresponding marginally compact conformation obtained in our calculations.

We point out that the results above, specific for  $N = 14$ , apply in general for ‘short’ thick polymers – ‘short’ here means less than approximately 20 – 30 monomers depending on the value of  $R_0$ . For longer tubes with thickness greater than  $R_0 = 0.8$ , the preferred ground state is one in which the different portions of the tube are parallel (see Fig.8). Indeed, this is expected to be, in the continuum, the ground state of a thick tube in the thermodynamic limit. The fact that section of the tubes in contact must position themselves parallel with respect with each other can be rationalized rather simply in the continuum model. Consider the interaction between two cylinders the points along whose axes are subject to a two-body potential as in Eq. 7. For thin tubes, the attraction roughly is substantially independent of the angle between the two axis, whereas for thicker tubes there is a marked minimum when the two axes are parallel to each other (see also the discussion in [9,57]). The resulting phase is similar to the nematic-like or crystalline polymer phases obtained with semiflexible polymers and reported recently in Refs. [58,59]. Our model is the first one, to our knowledge, to predict such a crossover between secondary structural motifs for short polymers and these nematic structures for long chains.

When the protein concentration in the cell is higher than a certain critical threshold, the proteins may misfold and aggregate to form amyloid fibers [60]. In the case of prions [30], for example, one observes a transition from  $\alpha$  to  $\beta$  rich structures which favours aggregation and causes bovine spongiform encephalopathy (BSE) disease in cattle. The shape of the aggregate can be visualized in a coarse grained way by thinking of different parts of the aggregate as portions of tubes which are aligned with respect to each other. Another classic example is that of DNA condensation in the presence of polyvalent counterions in solution. The globule structure formed by DNA upon condensation is usually a circular donut or spool with a hole in its interior when the DNA is short or its concentration is low (the stiffness of the double-stranded DNA molecule makes it energetically unfavourable to bend the tube sufficiently strongly to fill the hole) and a ‘nematic-like’ state with different portions of the molecule aligned along a local director, when the concentration is high [61]. The tube picture can not only explain the observed geometries but also the crossover between them on changing the tube length. If we postulate that the compact phase of a long tube is somewhat akin (due to the predominance of non-local contacts) to a concentrated phase of shorter tubes, our simulations could then qualitatively explain the experimental finding. Our recent simulations [11] confirm this expectation.

It is interesting to note that the zig-zag structures of planar configurations obtained for thickness  $R_0 \sim 1$  are not the same as found for  $\beta$ -sheets of proteins. In the latter case the zig-zag occurs perpendicular to the plane of the sheet. This geometry is a peculiarity of the detailed chemistry of the backbone and of the hydrogen bond. These peculiarities can also impact on the way proteins form amyloids which at the present time is not precisely known (see Ref. [62,63] for the most recent developments). However it is pleasing that the model proposed here is able to predict secondary motifs as shown in Fig. 6 (with the geometry of the helix exactly matching that of an  $\alpha$  helix) and at the same time amyloid-like phases for long proteins or ensembles of them.

We have previously shown that the thick polymer model defined via three body interactions admits a continuum limit without the need to regularize the potential. Such a continuum limit is attained by increasing the ratio  $R_0/b$ , where  $b$  is the distance between successive beads as in Section III. Hairpins and zig-zags would not be found in this limit as can be seen from Eq. 9 (which when the length  $b$  is different from 1 reads  $(R_1/b)^2 + 2 + \frac{R_1}{R_0} - 4(R_0/b)^2 = 0$ ), which in the continuum limit yields  $R_0 = R_1/2$  as the maximum thickness beyond which one cannot have contacts. When  $R_0 \lesssim R_1/2$  and the length of the

polymer is sufficiently short, the ground state is expected to be a space-filling helix, of the same kind as the one found in [6]. As the length increases, the ground state should cross over to a nematic-like structure in which different portions of the tube are straight and arranged on a triangular lattice when seen in a plane perpendicular to their axes.

### C. Ground states of short stiff chains

In this section we briefly study the nature of the ground states of a semiflexible polymer chain on increasing the stiffness. Our main aim is to understand the similarities and differences with the case of thick tubes. The system Hamiltonian is

$$H = \sum_{i < j} V(r_{ij}) - \kappa \sum_i \vec{r}_{i,i+1} \cdot \vec{r}_{i+1,i+2}, \quad (10)$$

where,  $V$  is the potential in Eq. 7, characterized by  $R_1 = 1.6$ ,  $R_{h.c.} = 0.55$ , and where  $\theta_i$  is the angle between consecutive bonds of the chain and  $\kappa$  is the bending rigidity.

In order to minimize the cost associated with the stiffness  $E_s = -\kappa \sum_{i=2}^{N-1} \cos \theta_i$ , conformations with a higher local radius of curvature are favoured, as is the case for tubes, for which local radii less than the tube thickness are forbidden. A key difference, however, is that in the semiflexible chain the stiffness term explicitly favors certain portions of phase space, whereas, in the flexible tube model, the thickness constraint merely forbids some regions of phase space, thereby implicitly favouring the remaining parts of phase space in a less direct way. As a result, the stiffness term is more effective in guiding the semiflexible polymer chain towards the ground state conformations, but the corresponding zoology of the ground state structures is not as rich as in the tube model. A crucial difference between a tube and a semiflexible chain model is in the non-local effects inherent in a tube description. Recall that in addition to constraints on the local radius of curvature, there is a strict requirement that none of the non-local triplets has a radius less than the tube thickness. This requirement leads to strong anisotropic interactions [57] between nearby tube segments in the marginally compact phase and is a feature that is entirely missing for a semiflexible chain. Just as found for the tubes, the semiflexible polymer exhibits a curve of the number of contacts versus stiffness (not shown) consisting of a series of plateaus.

In each of the plateaus, defined by a constant number of contacts and linearly increasing total energy, there is a unique ground state conformation, labelled from  $I$  to  $V$ , and shown in Fig. 9 (first row). One first obtains a kind of distorted ‘figure-eight’ hairpin ( $I$ ), possibly resembling the beginning of a double helix [64], for  $0 \leq \kappa \leq 2.4$ , then a ‘knot’ conformation ( $II$ ), for  $2.4 \leq \kappa \leq 4.6$ , a three-rod hairpin ( $III$ ) for  $4.6 \leq \kappa \leq 9.0$ , and a two-rod hairpin ( $IV$ ) for  $9.0 \leq \kappa \leq 10.9$ . In the last plateau ( $V$ ), for  $10.9 \leq \kappa \leq \infty$ , the ground state conformation is a straight stretched rod, with  $E_s = -12.0$ .

In contrast to the tube model, where the degeneracy of ground state conformations is reduced only at the end of each plateau, the semiflexible chain always has a unique ground state. In the latter case, there is no tuning of a relevant length scale (analogous to the tube thickness), which controls the degree to which the attractive two-body interaction can be availed of. On increasing the stiffness, one does not find either a marginally compact phase or a swollen phase. It is evident from conformation ( $IV$ ) that planarity in the semiflexible chain model arises merely from the need of having two straight stretched rods parallel to each other, whereas it is a more stringent geometrical requirement in the tube model. On the other hand, conformation ( $III$ ), is very similar to what we obtain for longer chains in the tube case. Indeed, we expect that, in the thermodynamic limit of chains of infinite length, the ground state, in both cases, is a nematic-like structure of long parallel rods filling the space with hexagonal symmetry. Unlike the tube, the stiff chain conformations (see, for example,  $II$  and the conformations in the last row of Figure 9) do not need to satisfy any non-local anisotropic constraints. Thus, in the latter case one expects a much higher degeneracy with a much greater number of alternative ground state conformations consisting of planes stacked onto each other with parallel (or antiparallel) alignment within the same plane, but not necessarily between different planes.

For low  $\kappa$  values, some of the simulations found conformations with portion of helices, or resembling helices of strands, as shown in Fig. 9, but they are never the ground state for any value of  $\kappa$ , and they are not as regular as in the tube case (compared e.g. to a long straight helix). Likewise, double helix conformation were found in the tube model but not as ground states.

Some preliminary results for longer chains ( $N = 22$ ) are also shown in the last row, which combine the main features of conformations ( $I$ ) and ( $II$ ) for  $N = 14$ , namely the winding around a central axis which is in turn formed by one end of the chain.

In the next section, we will present mean field calculations, complemented by Monte Carlo simulations, of the phase diagram of a tube in the thermodynamic limit.

## V. PHASE DIAGRAM OF A TUBE

Our goal, in this section, is to elucidate the phase diagram in the  $(T - R_0)$  plane, where  $T$  is the temperature and  $R_0$  is the thickness of a tube subject to an attractive pair potential of a given fixed range. We will do this by means of approximate analytic treatments which provide useful guideposts to a numerical attack on the problem. Taken together, these techniques provide a picture of the nature of the phases and the transitions between them.

It is useful, at the outset, to consider existing variants of the Edwards-like model of tethered spheres to understand what qualitatively new features are introduced in the tube picture. A commonly studied model discussed in the previous section is the stiff chain which starts with standard tethered spheres and introduces a curvature energy term in the Hamiltonian – the cost of local bending of the chain depends on the local radius of curvature and the sharper the local turn, the more expensive it is. The role of temperature in such a model is that at sufficiently high temperatures, sharp local turns are tolerated but as the temperature is lowered, such turns become harder to sustain and, indeed, one requires that the chain segments become straighter and straighter as the temperature is lowered. This local curvature effect may be captured in a potential energy of the form of Eq. 8, and leads to a schematic phase diagram in the  $(T-k)$  plane shown in Figure 10 [31,33].

In contrast, the tube picture has a somewhat different way of capturing local curvature effects. For a tube of thickness  $R_0$ , the local radius of curvature can be no smaller than  $R_0$ . A violation of this *temperature-independent* constraint would lead to a self-intersection of the tube and that would be prohibitively expensive. Thus, unlike the standard approach (see paragraph above) in which tube segments become locally straighter and straighter as the temperature is lowered, for a tube, certain conformations entailing tight local turns simply do not occur at any temperature.

The fact that different parts of the tube cannot intersect with each other (the triplet radii have to be greater than  $R_0$ ) leads to severe constraints on the nature of the interaction between tube segments. As described before, especially when the tube thickness is tuned (by hand or automatically, as in proteins) to be comparable to the range of the self-attraction, there are sharp constraints on the relative distance and mutual orientation of tube segments which must be met in order for the attractive interaction to be availed of. There are variants of the standard sphere model in polymer physics in which dangling ends are attached to the monomers and they interact via an anisotropic Maier-Saupe type of interaction commonly studied in the field of liquid crystals [65]. The tube picture may therefore be thought of as a new way of incorporating local curvature constraints along with a new variant of the anisotropic non-local interactions in a chain. Quite remarkably, these new variants result from elegant physical considerations of a very common every day object – a tube – and lead to new polymer physics and a unified explanation for the common characteristics of protein structures.

We proceed first to approximate mean field treatments of two variants of the tube model. The first is a chain of infinitesimal coins (each with a radius  $R_0$ ) and the second is the model with a three-body constraint which dictates that none of the triplet radii should be smaller than  $R_0$  (see eq. (6)). It is important to note that the mean field approximation does not take into account the tethering properly. As a result, in the case of the chain of coins neighbouring and non-neighbouring portions of the chains are considered to be equivalent, whereas in the second case, the non-local effects (giving self-avoidance) are neglected. Indeed, the formalism used in the mean field theory is technically similar to previous calculations with bending rigidity and liquid-crystal-like self interactions between the polymer beads (see e.g. [58,66]).

Armed with the insights from the approximate analytic analysis, we will embark on detailed Monte-Carlo simulations, which do not entail any approximations, to deduce the phase diagram.

### A. Mean field analysis

#### *The chain of coins*

Let us consider a chain of  $N$  infinitesimally thin coins, each having a radius  $R_0$ , whose centers are at  $\{\vec{r}_i\}_{i=1,\dots,N}$ . The coins cannot co-penetrate and they are subject to a pairwise purely attractive potential  $V_{2b}(\vec{r}_i - \vec{r}_j)$  whose argument is the distance between pairs of coin centers. We choose an isotropic 2-body potential promoting compaction in order to compare our results with those of the simulations in Section VB. The anisotropy arises from the geometrical shape of the constituents of the chain molecule. We postulate that the centers of the coin cannot approach each other closer than twice a given hard core radius  $R_{hc}$ . Thus one might think of the coins as being complemented by hard spheres whose center coincides with the coin center. This is necessitated in our mean field treatment in order to allow for a  $\Theta$  collapse – without the hard sphere, the free energy minimum would always correspond to a non-zero density and there would be no scope for the swollen phase. The partition function of this system at an inverse temperature  $\beta \equiv \frac{1}{T}$  is:

$$\mathcal{Z} = \int \prod_{i=1}^N d\vec{r}_i \prod_{i=1}^{N-1} \delta(|\vec{r}_{i+1} - \vec{r}_i| - 1) e^{\left(-\beta \sum_{i<j;i,j=1}^N V_{2b}(\vec{r}_i - \vec{r}_j)\right)} \prod_{i<j;i,j=1}^N (1 + f_{ij}^{(1)}) \prod_{i<j;i,j=1}^N (1 + f_{ij}^{(2)}), \quad (11)$$

where  $f_{ij}^{(1)}$  ( $f_{ij}^{(2)}$ ) is  $-1$  if the coins (spheres) centered in  $\vec{r}_i$  and in  $\vec{r}_j$  co-penetrate, and is  $0$  otherwise. We have taken the length of a link between two successive coins equal to  $1$ . We can also take  $\vec{r}_1 = \vec{0}$  without loss of generality.

We now introduce a density field  $\psi(\vec{r}, \vec{t})$ , where  $\vec{t}_i \equiv \vec{r}_i - \vec{r}_{i-1}$ , defined as follows:

$$\psi(\vec{r}, \vec{t}) = \sum_{i=2}^N \delta(\vec{r} - \vec{r}_i) \delta(\vec{t} - \vec{t}_i). \quad (12)$$

We proceed to expand the effective Hamiltonian in Eq. 11 in powers of  $f_{ij}^{(1),(2)}$  as in a standard virial expansion. By enforcing the definition in Eq. 12 through the introduction of a conjugate density field  $\hat{\psi}(\vec{r}, \vec{t})$ , and by restricting the virial expansion *in the free energy* to two particle clusters in  $f_{ij}^{(1)}$  and up to three particle clusters in  $f_{ij}^{(2)}$  (see the Appendix for more details on these steps), we can rewrite Eq. 11 as:

$$\mathcal{Z} = \int D\psi D\hat{\psi} \exp(-\mathcal{H}(\psi, \hat{\psi})) \quad (13)$$

where the explicit form of  $\mathcal{H}$  is given in the Appendix. From Eq. 13 one obtains the saddle point equations  $\delta\mathcal{H}/\delta\psi = \delta\mathcal{H}/\delta\hat{\psi} = 0$ . Solving these is equivalent to finding the optimal density configurations of the system, neglecting fluctuations. This means that we are making use of the mean field approximation. However an explicit solution is not possible without further simplifications. A very common one (used e.g. in Refs. [59,66]) consists of finding the solutions of the saddle point equations which have the form  $\psi(\vec{r}, \vec{t}) \equiv \rho\phi(\vec{t})$  and consequently one also has  $\hat{\psi}(\vec{r}, \vec{t}) \equiv \hat{\rho}\hat{\phi}(\vec{t})$ . While  $\rho$  represents the spatial density of particles, which is assumed to be uniform, the symbol  $\hat{\phi}(\vec{t})$  stands for the normalized probability that a link is oriented along the unit vector  $\vec{t}$ .

If we now use the self-consistent saddle point equations and insert them back into Eq. 13, we find that the mean field free energy functional per particle to be minimized is:

$$f_{mf}(\rho, \psi) = \int d\vec{t} \phi(\vec{t}) \log(\phi(\vec{t})) + \frac{1}{2}\beta \int d\vec{r} V_{2b}(\vec{r}) \rho + \frac{2}{3}\rho\pi R_{hc}^3 \quad (14)$$

$$+ B\rho^2 + 2\rho\pi R_0^3 \int d\vec{t} \int d\vec{t}' \left(1 - (\vec{t} \cdot \vec{t}')\right)^{\frac{1}{2}} \phi(\vec{t})\phi(\vec{t}');$$

where the first term is the entropy contribution from the chain constraint, the next three terms arise from the two-body potential (the first is the attractive interaction and the other two are the repulsive terms and are responsible for obtaining a  $\Theta$  transition in our theory), whereas the last term is the coin excluded volume mean field interaction which encapsulates the anisotropy in the model [67], and where  $B \equiv \frac{8\pi^2 \rho^2}{3} \int_0^{R_{hc}} dr_1 \int_0^{R_{hc}} dr_2 \int_{-1}^1 d\cos\theta r_1^2 r_2^2 H(R_{hc}^2 - r_1^2 - r_2^2 + 2r_1 r_2 \cos(\theta))$  as shown in the Appendix. In the last formula  $H(x)$  is  $0$  if  $x < 0$  and  $1$  otherwise. It is noteworthy that the qualitative form of the resulting phase diagram (see below and Fig. 11), does not depend on the numerical value of  $B$ , but just on its presence and on it being greater than  $0$  in order to render the density of the globule finite when the system is in the compact phase.

We now have to minimize Eq. 14 with respect to  $\rho$  and  $\phi$ . We define  $\int d\vec{r} V_{2b}(\vec{r}) \equiv -V_0$ , which is the only feature of the pair-wise attractive potential which affects the mean field solution. When  $T$  is high ( $\beta$  is small), the minimum of  $f_{mf}$  occurs for  $\rho = \psi(\vec{t}) = 0$ : this is the isotropic, swollen phase. At a critical value of the temperature given by  $\beta_{\Theta} = T_{\Theta}^{-1} = \frac{\frac{2}{3}R_0^3 + \frac{4}{3}\pi R_{hc}^3}{V_0}$ , there is a phase transition into a phase with  $\rho \neq 0$  and  $\phi = 0$ , which is physically an isotropic, globular phase. This transition is second order within the mean field approximation ( $\rho \propto (\beta - \beta_{\Theta})$  as  $\beta \rightarrow \beta_{\Theta}^+$ ). If  $T$  is further lowered, we find a second phase transition to an anisotropic, globule phase (with non-zero orientational order parameter  $\phi$ ) at a temperature:

$$T = T_F = \frac{T_{\Theta}}{1 + \frac{BT_{\Theta}}{R_0^3 V_0}} \quad (15)$$

Eq. 15 was derived by mapping our theory onto the liquid crystal theory discussed in Ref. [68] (see Section II of that work and in particular Eqs. 18 and 27). Another possible way to obtain the phase boundary is via the use of Onsager's trial functions [67]. (A similar procedure can also be carried out for the semiflexible chain model.) This is a first order transition since the order parameter, which is the average of the second Legendre polynomial with respect to  $\phi(\vec{t})$ , displays a jump at this transition. This transition is qualitatively similar to the transition found in Ref. [69] with a fluid of hard discs. Note that the ratio between the two transition temperatures,  $T_F/T_{\Theta}$  (see Eq. 15) approaches  $1$  for large  $R_0$  as  $1 - \frac{a}{R_0^3}$ , with  $a > 0$  a constant.

The precise form of the phase diagram is shown in Figure 11, top panel. A qualitatively similar phase diagram is to be expected if the chain of coins is replaced by a chain made up of objects with an inherent asymmetry in their geometry, such as e.g. a cylinder. There are two distinct regimes as a function of tube thickness: the first is one in which the tube is ‘thin’, which occurs when  $R_0 < 1.5$  roughly, and in which there are two transitions as  $T$  decreases, the first (the usual  $\Theta$  transition) from the coil to the globule phase, and the second, which we shall call a ‘folding transition’, between an isotropic globule and a compact configuration in which there is orientational order. In this low temperature phase, the ground state of the chain of coins resembles the lamellar semi-crystalline polymer phase and the ground state of the long thick polymer (Figure 8) discussed in the previous section.

The second regime is when the thickness  $R_0$  is larger than 1.5: we can think of this as the ‘thick tube’ case. In this second regime there is practically only one transition, i.e. the temperature range over which one observes the isotropic, globule phase is vanishingly small. Indeed, we expect that the very existence of this phase for thick tubes is an artifact of our mean field approximation. A similar situation was observed in References [31,66] in which two transitions were predicted in the mean field approximation for stiff polymers whereas simulations indicate that the true solution should display a single first order transition. There is evidence from experiments and recent theoretical results on the thermodynamics of proteins [70,71] that they may undergo either only one single folding transition or a  $\theta$ -collapse followed by a distinct folding transition at a lower temperature. This suggests that both cases, corresponding to thin and thick tubes, are found in protein thermodynamics. We conclude with the observation that the absence, in our analysis, of a swollen phase for very thick tubes at zero temperature, contrary to expectations based on common sense considerations that the attractive interactions cannot be availed of when the tube is too thick, is an artifact of the mean field approximation.

We now briefly compare the phase diagram resulting from the mean field approximation in our model with that in Fig. 10, stemming from the corresponding approximation in the stiff polymer model. The three main phases present in both cases are the same. There is however a notable difference in the phase boundary shape. For the tube, there is a transition at low  $T$  between the anisotropic globule and swollen phases on inflating the tube. In contrast, for a stiff chain, unless the bending rigidity penalty is infinite at zero temperature one is always in the compact phase. Furthermore, the collapse of stiffer chains occurs at higher  $T$ , while that of thicker tubes occur at lower  $T$ .

#### *The tube with a three-body radius constraint*

We briefly give the results of the same mean field treatment applied to a tube-like polymer with a three body constraint (see preceding section). Here once more the suitable order parameters are  $\rho$ , the density, and  $\phi(\vec{t})$ , the link orientational order parameter. We have also considered the presence of a standard two-body hard core which prevents the transition temperature from being infinity, when one has a vanishingly thin tube i.e. when  $R_0 = 0$ . The phase diagram is shown schematically in Figure 11, bottom panel. Unlike the chain of coins, there is no region in which there are two transitions. The transition temperature is  $T_\Theta = \frac{V_0}{2B(R_0) + \frac{4}{3}\pi R_{hc}^3}$ , where  $B(R_0) \equiv \frac{1}{V} \int \int d\vec{r}_1 d\vec{r}_2 d\vec{r}_3 f_3(\vec{r}_1, \vec{r}_2, \vec{r}_3) \delta(|\vec{r}_3 - \vec{r}_2| - 1)$ , which goes to  $\infty$  as  $R_0 \rightarrow \infty$ . In this formula  $f_3$  is 0 if the radius of the circle constructed with the triplet  $\vec{r}_{1,2,3}$  is greater than  $R_0$  and  $-1$  otherwise: this term acts as an effective thickness-dependent two-body hard core.  $V$  is the volume occupied by the system in the canonical ensemble. The  $\Theta$  collapse is from a swollen phase to an isotropic globule if  $R_0 < \frac{1}{2}$ , and to an anisotropic globule otherwise. There is a transition from the thin tube to the thick tube limit at low temperatures as the thickness increased past  $R_0 = 1/2$ . Unlike the chain of coins, the transition is second order in both cases. It is interesting to note that that the worm-like chain model [72], eq. (9), subject to a potential, which promotes compaction, would yield a qualitatively similar phase diagram in the mean field approximation. This is so because, in first order in the cluster expansion, the tube is important only in disallowing strong bends as happens also for polymers with stiffness. This also explains why the boundary between thin and thick tubes is located at  $R_0 = 1/2$ : the local constraint on the bending angle imposed by the thickness is given by  $\vec{R}_{i,i+1} \cdot \vec{R}_{i+1,i+2} \geq 1 - 1/(2R_0^2)$ , and there is no restriction for  $R_0 < 1/2$ . Indeed, the configuration of two neighbouring links being exactly superimposed corresponds to a local thickness which is  $1/2$ . However, higher order terms in the virial expansion, that have not been considered here, would begin to capture the non-local thickness effects when different portions of the tube come into contact with one another. This results in differences between the tube constraint and the worm-like chain model and also alters the threshold value between the thin and thick tube limits.

Even though the local constraint in our mean field is not the full story and does not properly begin to capture the self-avoidance imposed by non-local constraints, it already allows one to identify an important difference between our model and the worm-like chain when the continuum limit is approached. From the inequality  $\vec{R}_{i,i+1} \cdot \vec{R}_{i+1,i+2} \geq 1 - 1/(2R_0^2)$ , one can infer after some standard algebra that, in the swollen phase, the persistence length of a tube of thickness  $R_0$  scales as  $R_0^2/b$  as  $b \rightarrow 0$  (see Ref. [73] for a calculation of the persistence length of a thick polymer applied to the case of double-stranded DNA molecule). This is connected to the fact that the local tangent to the tube axis is continuous and differentiable and thus the axis (centerline) of the continuum tube is twice differentiable, whereas the curve corresponding to the continuum limit of a semiflexible polymer is only differentiable once. This means that the thick polymer model can be of use in cases in which all three Frenet vectors need to be defined in the continuum limit.

The mean field calculations provide us with useful insight on what kinds of phases one might expect, the possibility of qualitatively distinct behaviors of thin and thick tubes and the possibility in some cases for two transitions on lowering the

temperature starting from the high temperature swollen phase. Armed with this information, we now proceed to careful Monte Carlo simulations, which are not subject to the approximations used in the mean field calculations.

## B. Monte-Carlo evaluation of the phase diagram

We now consider a tube of a given thickness, schematized as explained above with a three body effective constraint. The methods employed are Monte-Carlo simulations, with the parallel tempering or multiple Markov chain technique (see [74]). A number of replicas (from 11 to 16 in our simulations) of the polymers are equilibrated simultaneously at different temperatures, allowing the possibility of two replica neighbours in  $T$  to exchange their configurations after a fixed number of steps. In all formulas below,  $\langle \cdot \rangle$  denotes ensemble averaging. For each thickness considered, we calculate the specific heat  $C$  using

$$C(T, R_0) = \beta^2 (\langle E^2 \rangle - \langle E \rangle^2), \quad (16)$$

where  $E$  is the internal energy (contact number) and  $\beta \equiv \frac{1}{T}$  is the inverse temperature. The radius of gyration  $R_g$  is defined by

$$R_g(T, R_0) = \left\langle \frac{\sum_{i=1}^N (\vec{r}_i - \vec{r}_{cm})^2}{N} \right\rangle^{1/2}, \quad (17)$$

where  $\{\vec{r}_i\}_{i=1, \dots, N}$  represent the coordinates of the  $N$  beads and  $\{\vec{r}_{cm}\}$  the coordinates of the center of mass of the tube.

We also record three probability distributions: the distribution of the chirality  $\chi$ , which is a number between  $-1$  and  $1$  defined for every consecutive quadruplet of beads along the chain by

$$\chi \equiv \vec{r}_{i,i+1} \cdot (\vec{r}_{i+1,i+2} \times \vec{r}_{i+2,i+3}); \quad (18)$$

the distribution of  $\cos(\theta)$ , where  $\theta$  is the angle between consecutive links along the chain; and that of  $\cos(\xi)$  where  $\xi$  is the angle between two links which are in contact. Note that the distance between successive beads is held fixed at unity and two links  $(\vec{r}_{i+1} - \vec{r}_i$  and  $\vec{r}_{j+1} - \vec{r}_j)$  are defined to be in contact when  $|\vec{r}_i - \vec{r}_j| < R_1$ . We label these probability distributions  $P(\chi)$ ,  $P(\cos(\theta))$  and  $P(\cos(\xi))$  respectively. For comparison, it is useful to note the shapes of these distributions for a non-interacting random walk:

$$P(\chi) \propto \arcsin\left(\sqrt{1 - \chi^2}\right) \quad (19)$$

$$P(\cos(\theta)) \equiv P(\cos(\xi)) \equiv \text{const.}$$

As with all Monte Carlo algorithms, finding canonical averages and particularly the specific heat at low temperatures is difficult. The multiple Markov chain (or parallel tempering) algorithm helps alleviate this difficulty by enhancing the mobility of the chain at low  $T$ . To further improve the results at low  $T$ , we first performed one or more parallel tempering runs collecting data for the canonical averages, the specific heat and the low  $T$  configurations, starting from an open initial condition (more or less straight chains are chosen for all the replicas). Then another run is performed with the replicas starting from a ‘folded’ conformation, the one with the minimum energy found in the preceding runs. The latter approach allows one to sample more accurately the low  $T$  configurations, giving a bias towards the ‘correct’ ground state at very low  $T$ . We have verified that the high  $T$  behaviour is the same for all runs.

Figure 12 shows the phase diagram in the  $(T, R_0)$  plane and confirms the mean field prediction of two quite distinct regimes, one for thin tubes and the other for thick tubes with the boundary separating them being  $R_0 \sim 0.8$  for the parameters used in the simulation. Figures 13 and 14 show the behaviour of the specific heat and of the radius of gyration for two different thickness values, typical of thin ( $R_0 = 0.7$ ) and thick ( $R_0 = 0.95$ ) tubes. Figures 15-20 show typical histograms for  $P(\chi)$ ,  $P(\cos(\theta))$ ,  $P(\cos(\xi))$ . We considered polymers with  $N = 20, 41$  and  $60$  and performed Monte-Carlo runs scanning the thickness  $R_0$  in steps of  $0.05$  units.

### *Regime 1: Thin tubes*

In many respects, the thermodynamic behavior of thin tubes is similar to that reported in Ref. [51], which was meant to describe conventional polymers of zero thickness. Here we will describe the behavior of a tube of thickness  $R_0 = 0.7$  as representative of the thin tube regime. Figure 13 shows a scaling plot of the radius of gyration versus temperature. Note the nice intersection of the three curves at  $T_\Theta = 1.5$  with the standard scaling of  $R_g \sim N^{1/2}$  based on the expectation of  $\nu = \nu_\theta = 1/2$ . The specific heat however displays a peak only for  $T$  approximately equal to  $1$  (see the somewhat noisy Figure 13), a value

significantly smaller than the previous one. The data are suggestive of another transition at a lower temperature.

The  $P(\chi)$  histogram is more strongly peaked around  $\chi = 0$  than one would expect for the random walk case in the swollen phase. In the isotropic globule phase, along with the drop in the radius of gyration, one observes a somewhat flatter distribution, which persists down to the lower temperature peak in the specific heat at which point a multi-peaked histogram of  $\chi$  is obtained. The analysis of the distribution of the cosine of the angle  $\theta$  between successive links suggests that, at high  $T$  (in the swollen phase) it is almost flat as expected from random walk considerations. In the isotropic globular phase, values of  $\cos(\theta)$  corresponding to local tube segments which are not tightly bent are penalized; at the lowest temperature shown, this effect is more pronounced (and two peaks develop for small values of  $\cos(\theta)$ ). Strikingly, at temperatures below the ‘ $\Theta$ -like’ transition, the values of  $\cos(\theta)$  which are not penalized correspond to a local thickness roughly between 0.7 (the constraint imposed by the tube) and slightly more than 0.8 – it is as if ‘locally thin’ tubes only dominate the thick polymer distribution probability after the  $\Theta$ -like collapse. It is interesting to note that, with  $R_1 = 1.6$ , in order for beads  $i$  and  $i + 2$  to make contacts, it is necessary that  $R_0 < 0.83\dots$ , which is close to the thick threshold size. Finally, the  $P(\cos(\xi))$  histogram shows that the lower temperature peak in the specific heat is associated with a mild increase in the probability of contacts to occur between anti-parallel and parallel links.

In Ref. [51] it was suggested that, in a model similar to ours without the tube constraint, on lowering the temperature, first, there is a  $\Theta$  transition from the coil to the globule phase, equivalent to the usual gas-to-liquid transition. This is signalled by a drop in the radius of gyration as well as by a shoulder in the specific heat. Subsequently, the globule crystallizes (as in a liquid-to-solid transition for clusters of hard spheres) giving rise to the first peak in the specific heat. This is a first order transition in contrast to the second-order transition of the standard  $\Theta$  collapse. Finally, there is a third transition, which the authors refer to as a solid-to-solid first order transition. Exact enumerations [75] of interacting self-avoiding walks on a two-dimensional lattice suggest a similar behavior with a drop in the radius of gyration at a higher  $T$  than the one at which the specific heat displays a peak, and at a yet lower  $T$  one finds a second specific heat peak.

It is our belief that the thermodynamics of a thin tube is similar to that proposed in Ref. [51] up to the first specific heat peak. At lower temperatures, the cylindrical shape of the tube leads to different behavior. Our numerical evidence is somewhat weak on whether the second specific heat peak corresponds to a physical transition. In any case, we expect that such a transition, if it existed, would be different from the solid-to-solid transition postulated for polymers.

#### *Regime 2: Thick tubes*

For larger thicknesses (roughly from  $R_0 = 0.8$  upwards), the thermodynamic behaviour is different. In this case, the point in which the scaled curves for  $R_g$  intersect and the location of the peak in the specific heat (see Figure 14) are not very different as it was in the case of thin polymers. This suggests that in this case there is a single transition. Also the data for the specific heat per monomer, within the Monte-Carlo errors, suggest that this quantity diverges at the transition linearly with the chain length. We thus predict that this is a first order direct transition from a swollen phase to a ‘nematic-like’ globular phase. This prediction is in agreement with the mean field analysis of the preceding subsection and is also confirmed by other data (see below). That the low temperature phase is indeed characterized by segments of the tubes trying to position themselves parallel or anti parallel with respect to each other is clear from the distribution  $P(\cos \xi)$ , which, at low  $T$ , has sharp peaks around  $-1$  and  $1$ . As is the case for the continuum ground state of long tubes, one may conjecture that for long tubes the ground state will have tube segments aligned with respect to one another similar to the Abrikosov flux lattice, as in Figure 8. It should be noted that the segments of the tubes which face each other are more or less straight only for tubes that are not too thick (around  $R_0 = 0.9$  in our simulations, see Figure 8). For larger tube thickness, the thickness constraint leads to an absence of a peak in the distribution  $P(\cos(\theta))$  around  $1$  (See Figure 19). The analysis of  $P(\chi)$  (Figure 18) reveals that at high  $T$  the chirality distribution is wedge-shaped, so the peak at  $\chi = 0$  is more enhanced with respect to the case of low thickness. This shape persists almost up to the transition point, and there are no pre-transition effects as in the thin polymer case, consistent with a sharp first order transition. Below the transition, three moderate peaks develop, one for  $\chi = 0$ , which is not present for  $R_0 = 0.7$ , and the other two roughly symmetrically at the edge of the  $\chi$  spectrum visited by the system. The central one likely originates from planar or quasi-planar structures in the sampled configurations – a planar structure has  $\chi = 0$ .

The scaling collapse of the radius of gyration data are consistent with both  $\nu = \frac{1}{2}$  as in the standard  $\Theta$  point transition and  $\nu = 0.588\dots$  as would pertain to a first order transition with coexistence at the transition point (the exponent of polymers in the swollen phase). It is interesting to note that at the critical value of  $R_0$  at zero  $T$  (precisely  $R_0 = 1.2124\dots$ ), one obtains, as the ground state, compact configurations in  $d = 2$  whose  $\nu = \frac{1}{2}$ .

Strikingly, the ‘triple point’ in the phase diagram (Figure 12), which separates the ‘thin’ and ‘thick’ tube regimes (corresponding to a tube thickness of around 0.8) coincides with the thickness corresponding to the onset of the marginally compact region in the minima analysis for short polymers detailed in Section III. It is instructive to compare the phase diagram in Figure 12 with that of a stiff polymer (Figure 10) with no thickness (see e.g. Ref. [31,33,66]). Stiff polymers are known to undergo either two transitions, one second and the other first order, or only one first order transition, according to whether the



stiffness is small or high. The thickness of our tube prevents it from having sharp bends and this is reflected in the tube having a bigger persistence length than a polymer with no thickness: in other words, the thickness acts *locally* as a stiffness. However, the thickness also has an important non-local role both in providing a simple mechanism through which distant portions of the polymers must orient themselves selectively in order to take advantage of attractive interactions, and, more important, in providing a natural way in which secondary motifs such as helices and sheets arise with no need of heterogeneity in the model. As we discussed above, no such secondary structures appear in the resulting ground states of stiff polymers, whereas with thick polymers we obtain both  $\alpha$  helices and  $\beta$  sheets. Also, thick discrete polymers display a planar phase at high values of the thickness which does not happen for stiff polymers.

We have also performed an analysis of the ‘unfolded state’, i.e. of the *ensemble* of tube configurations in the swollen phase at temperatures just above the transition. Again the situation is different for thin tubes and thick tubes. In the former case, the unfolded state is one in which some contacts are already formed, though with no regularity typical of the crystalline phase. In the latter case, on the other hand, consistent with the fact that the transition is found to be first order, we observe that just above the transition point the chain is still indistinguishable from a typical configuration in the swollen phase. This is supported by a study of the  $P(\cos \xi)$  distribution – for a thick tube, there are no precursors to the transition (see Figure 20). This confirms, as is observed in small proteins, that the folding transition is sharp or an all-or-none kind.

*Regime 3: Very thick tubes*

We can finally identify, in our Monte Carlo simulations, a regime not found in the mean field calculations of a swollen phase corresponding to very thick tubes. As expected from physical considerations, very thick tubes ( $R_0 > 1.2124 \dots$ ) are unable to avail of the attractive interactions and one obtains a swollen phase at all temperatures. This is in contrast to our mean field result within which the threshold thickness was essentially infinity. Note that such a swollen phase does not occur for chains with a bending energy constraint.

## VI. CONCLUSIONS

In summary, we have introduced the concept of a thick polymer and have studied the phase behaviour of such tubes. A key point to describing tubes is the need to have a three body constraint for ensuring that the local radius of curvature is not smaller than the tube thickness and that the tube does not self-intersect. Such a description deftly avoids the need for a singular interaction energy in the continuum limit as is the case with the classic Edwards model. There are three regimes of tube thicknesses (measured as a ratio of the thickness to the range of the self-attraction) with distinct phase behaviours. Generally, the categorization of a given polymer chain, in terms of the corresponding thickness regime, will crucially depend on its specific stereochemical properties, and the tube thickness may well not be a relevant physical parameter in some cases. On the other hand, there are cases, such as proteins, where the presence of bulky side chains attached to the main backbone naturally calls for a tubelike description. Indeed, the intermediate thickness regime leads to space-filling marginally compact conformations and for short tubes the ground state structures are helices and planar sheets with the same geometry as in secondary motifs in proteins. Moreover, this phase has many advantages associated with it which are exploited by nature housing biomolecular structures in it. The tube picture provides a natural way of connecting conventional polymer phases with the biomolecular phase.

We have also compared the ground states and the thermodynamics of a short tube with those of a chain of spheres with a non-zero stiffness (worm-like chain model in its continuum version). No secondary structures and no planar ground state structures appear, in general, for the stiff polymer model, as demonstrated in our computational analysis of short chains. Also, while stiff polymers can undergo two different transitions on varying the temperature for certain values of the bending rigidity parameter, they do not exhibit a swollen phase at zero temperature as does a fat tube. Furthermore, thick polymers not only provide an elegant explanation for the novel phase selected by Nature to house biomolecular structures but also provide a smooth link between this phase and conventional polymer phases. More fundamentally, the tube picture incorporates the anisotropy inherent in any chain model and provides the simplest geometrical construction that captures the essential features of any chain molecule.

On increasing the length of the polymer, or the number of polymer chains, there is some similarity between the tube picture and the worm-like chain model. When the tube is longer, we observe, in computer simulations, a crossover to semi-crystalline structures with different portions of the backbone chain lying parallel to one another. Our mean field analysis yields a phase diagram in the thermodynamic limit which is somewhat similar to the stiff chain phase diagram (see Fig. 10,11). There are clear differences as well arising from the fact that local distortions with a radius of curvature less than the tube thickness are disallowed for a flexible tube, whereas, for a stiff chain, there is an increasing penalty as the temperature is lowered and the local bending increases. Moreover, and most significantly, the connection with the biomolecular phase present in the phase diagram of short tubes allows us to rationalize the ubiquitous formation of amyloid fibrils in misfolded proteins as a biopolymer crystalline phase.

The simplified thick polymer model presented here does not, of itself, lead to tertiary arrangement of elements of local secondary structure. We have recently shown [10,11] that this likely arises from the geometrical constraints imposed by hydrogen bonds.

Another intriguing direction for future research is to consider the role of amino-acid heterogeneity in the two body potential, which is well known to play an important role in determining the folded structure of a polypeptide (see e.g. Ref. [76] and references therein). An extension of ideas presented here can be used to describe surfaces of non-zero thickness. Such a description entails the use of 4-body potentials [47]. An exploration of the phase diagram of such systems, which are relevant to membranes and surfaces, is likely to yield novel and rich behaviour as well.

*Acknowledgments:* We are indebted to Trinh Hoang, Sanat Kumar and Flavio Seno for stimulating discussions. This work was supported by MURST, cofin2003, NASA, NSF (DGE-9987589) and the Penn State MRSEC under NSF grant DMR-0080019.

- 
- [1] Flory, P. J., *Statistical mechanics of chain molecules*, Wiley, New York, 1969.
  - [2] Pauling, L., Corey, R. B. and Branson, H. R., *Proc. Natl. Acad. Sci. USA* **37**, 205-211 (1951).
  - [3] Pauling, L. and Corey, R., B., *Proc. Natl. Acad. Sci. USA* **37**, 729-740 (1951).
  - [4] Chothia, C., *Nature* **357**, 543 (1992).
  - [5] Stasiak, A., Maddocks, J. H., *Nature* **406**, 251 (2000).
  - [6] Maritan, A., Micheletti, C., Trovato, A. and Banavar, J. R., *Nature* **406**, 287-290 (2000).
  - [7] Banavar, J. R. and Maritan, A., *Rev. Mod. Phys.*, **75**, 23 (2003).
  - [8] Banavar, J. R., Maritan, A., Micheletti, C. and Trovato, A., *Proteins* **47**, 315 (2002).
  - [9] Banavar, J. R., Flammini, A., Marenduzzo, D., Maritan, A., Trovato, A., *ComPlexUs* **1**, 4 (2003); Banavar, J. R., Flammini, A., Marenduzzo, D., Maritan, A., Trovato, A., *J. Phys.: Condens. Mat.* **15**, S1797 (2003).
  - [10] Hoang T. X., Trovato A., Seno F., Banavar, J. R. and Maritan A., *Proc. Natl. Acad. Sci.* **101**, 7960 (2004).
  - [11] Banavar, J. R., Hoang, T. X., Maritan, A., Seno, F., Trovato, A., *Phys. Rev. E*, in press (2004).
  - [12] Bouchiat, C., Mezard, M., *Phys. Rev. Lett.* **80**, 1556 (1998).
  - [13] Moroz, J. D., Nelson, P., *Macromolecules* **31**, 6333 (1998).
  - [14] Dill, K. A. *Protein Sci.* **8**, 1166 (1999).
  - [15] Doi, M., and Edwards, S. F., *The theory of polymer dynamics*, Clarendon Press, New York, 1993.
  - [16] Flory, P. J. *Proc. R. Soc. London, Ser. A* **234**, 60 (1956).
  - [17] The concept of thickness has been introduced by Buck and Orloff in the context of ideal knots. Buck, G, and Orloff, J., *Topol. Appl.* **61**, 205 (1995).
  - [18] Elias, H.-G., *Macromolecules, Vol. 1: Structure and Properties*, 2nd edition, Plenum Press, New York and London (1984).
  - [19] Gonzalez, O. and Maddocks, J. H., *Proc. Natl. Acad. Sci. USA* **96**, 4769 (1999).
  - [20] In a different context, recent studies [22–24] have underscored the importance of the range of the attractive interactions in determining the stability of the fluid-fluid coexistence curve in a system of hard spheres and the importance of anisotropy in determining the phase diagram of protein solutions.
  - [21] Note that models different from ours but incorporating anisotropy of the chain backbone have been proposed for discrete polymer chains in the past (see Refs. [25–29] for some examples). Our model however allows one to take the continuum limit without introducing further cut-offs in the theory.
  - [22] ten Wolde, P.-R., Frenkel, D., *Science* **277**, 1975 (1997).
  - [23] Lomakin, A., Asherie, N., Benedek, G. B., *Proc. Nat. Acad. Sci.* **96**, 9465 (1999).
  - [24] Kern, N., Frenkel, D., *J. Chem. Phys.* **118**, 9882 (2003).
  - [25] Odijk, T., *Macromolecules* **19**, 2313 (1986).
  - [26] Khoklov, A. R., Semenov, A. N., *Macromolecules* **19**, 373 (1986).
  - [27] Stroobants, A., Lekkerkerker, H. N. W., Odijk, T., *Macromolecules* **19**, 2232 (1986).
  - [28] Odijk, T., *Macromolecules* **25**, 5533 (1992).
  - [29] Semenov, A. N., Nyrkova, I. A., Khokhlov, A. R., *Macromolecules* **28**, 7491 (1995).
  - [30] Prusiner, D. B., *Proc. Natl. Acad. Sci. USA* **95**, 13363 (1998).
  - [31] Doniach, S., Garel, T., Orland, H., *J. Chem. Phys.* **105**, 1601 (1996).
  - [32] Bhattacharjee, S. M., Muthukumar, M., *J. Chem. Phys.* **86**, 411 (1987).
  - [33] Lise, S., Maritan, A., Pelizzola, *Phys. Rev. E* **58**, R5241 (1998).
  - [34] des Cloiseaux, G. and Jannink, J. F., *Polymers in solution: their modeling and structure*, Clarendon Press, Oxford, 1990.
  - [35] Yamakawa, H., *Modern theory of polymer solutions*, Harper and Row, New York, 1971.
  - [36] de Gennes, P. G., *Scaling concepts in polymer physics*, Cornell University Press, Ithaca, 1979.

- [37] One can formally map the model in eq. (1) into a field theory of an  $n$ -component field,  $\vec{\phi}(\vec{x})$ . In the grand canonical formulation with a fugacity per unit length,  $r$ , the Hamiltonian of the field theory is given by

$$H_n(\{\phi\}) = \int d^d x \left\{ \frac{1}{2} \partial_\mu \vec{\phi} \partial_\mu \vec{\phi} + r \vec{\phi}^2 + \sum_m \frac{v_m}{m!} (\vec{\phi}^2)^m \right\} \quad (20)$$

Correlation functions for the corresponding polymer model are calculated from the  $\vec{\phi}$  correlation in the  $n \rightarrow 0$  limit [38,39]. The renormalizability of such a field theory is well known and it is guaranteed that, from a perturbative expansion, one can extract results which depend only on a finite number of parameters.

- [38] de Gennes, P. G., *Phys. Lett. A* **38**, 339 (1972).
- [39] Zinn-Justin, J., *Quantum field theory and critical phenomena*, (3rd edition, Oxford, University Press) (1996).
- [40] Barrett, A. J., Domb, C., *J. Stat. Phys.* **77**, 491 (1994).
- [41] Grosberg, A. Y., *Phys. Rev. Lett.* **85**, 3858 (2000).
- [42] Dobay, A., Dubochet, J., Millett, K., Sottas P. E., and Stasiak A., *Proc. Natl. Acad. Sci. USA* **100**, 5611 (2003).
- [43] Nelson, D. R., Piran, T. and Weinberg, S., Editors, *Statistical mechanics of membranes and surfaces*, Volume 5 of Jerusalem Winter School for Theoretical Physics, World Scientific, Singapore, 1989.
- [44] Wiese, K. J., *Polymerized membranes, a review*, in Phase transitions and critical phenomena, Vol. 19, edited by Domb, C. and Lebowitz, J. L., Academic Press, New York, 2000.
- [45] An interesting problem for thick polymers in the continuum limit is the measure associated with the curve corresponding to the viable centerline of a thick tube. Indeed, for the Edwards model, the first term in the effective energy in Eq. (1) is used to define a measure on the ensemble of all continuous curves embedded in three-dimensional space, the Wiener measure. It is well known that this gives a non-zero weight to all curves which are continuous but not differentiable ( $C^0$  curves in the standard notation)). In particular, the curves for which the tangent can be defined are a subset of zero measure in this ensemble. It can be proved rigorously (see e.g. Ref. [46]) that if a curve is a viable centerline for a tube of non zero thickness, then it must satisfy more stringent smoothness requirements, namely it should be  $C^{1,1}$ , i.e. it is differentiable and its derivative is a Lipschitz function (see [46] and Refs. therein). An interesting problem, which we do not consider here, is the definition of a suitable measure in the continuum limit for such thick polymer centerlines. One possibility is, of course, to add, to the first term in Eq. (1), the three body potential introduced in this work defined for all possible triplet radii, but this, for the reason just mentioned, does not lend itself to a straightforward perturbative formulation.
- [46] Gonzalez, O., Maddocks, J. H., Schuricht, F., von der Mosel, H., *Calc. Var. Partial Dif.* **14**, 29 (2002).
- [47] Banavar, J. R., Gonzalez, O., Maddocks, J. H. and Maritan, A., *J. Stat. Phys.* **110**, 35 (2003).
- [48] C. Vanderzande, *Lattice models of polymers*, Cambridge University Press, U.K. (1998).
- [49] Pronk, S., Frenkel, D., *J. Chem. Phys.* **110**, 4589 (1999).
- [50] Mau, S. C., Huse, D. A., *Phys. Rev. E* **59**, 4396 (1999).
- [51] Zhou Y. Q., Karplus M., Wichert J. M., Hall C. K., *J. Chem. Phys.* **107**, 10691 (1997).
- [52] Wang, F. G., Landau, D. P., *Phys. Rev. Lett.* **86**, 2050 (2001).
- [53] We call a tube space filling if the smallest convex set which contains it (its convex hull) is simply connected, i.e. has no holes at its interior.
- [54] Allain, F. H. T., Yen, M., Masse, J. E., Schultze, P., Dieckmann, T., Johnson, R. C. and Feigon, J., *Embo J.* **18**, 2563 (1999).
- [55] Chang, K. Y. and Tinoco, I., *J. Mol. Biol.* **269**, 52 (1997).
- [56] Baumann, U., Wu, S., Flaherty, K. M. and Mckay, D. B., *Embo J.*
- [57] Banavar, J. R., Maritan, A. and Seno, F., *Proteins* **49**, 246 (2002).
- [58] Ghosh, K., Carri, G. A., Muthukumar, M., *J. Chem. Phys.* **116**, 5299 (2002).
- [59] Welch, P., Muthukumar, M., *Phys. Rev. Lett.* **87**, 218302 (2001).
- [60] Dobson, C. M. *Nature* **418**, 729 (2002). **12**, 3357 (1993).
- [61] Bloomfield, V. A., *Biopolymers* **44**, 269 (1997).
- [62] Perutz, M. F., Finch, J. T., Berriman, J., Lesk, A., *Proc. Natl. Acad. Sci. USA* **99**, 5591 (2002).
- [63] Petkova, A. T., Ishii, Y., Balbach, J. J., Antzutkin, O. N., Leapman, R. D., Delaglio, F., Tycko, R., *Proc. Natl. Acad. Sci. USA* **99**, 16742 (2002).
- [64] Looking at the conformation with the chain not drawn it is evident that the balls are sitting on the sites of a regular lattice, possibly *fcc*.
- [65] Maier, W., Saube, A. Z., *Naturforsch.* **A13**, 564 (1958).
- [66] Pitard, E., Garel, T., Orland, H., *J. Phys. I* **7**, 1201 (1997).
- [67] Onsager, L. *Ann. NY Acad. Sci.* **51**, 627 (1949).
- [68] Vroege, G. J., Lekkerkerker, H. N. W., *Rep. Prog. Phys.* **55**, 1241 (1992).
- [69] Frenkel, D., Eppenga, R., *Phys. Rev. Lett.* **49**, 1089 (1982).
- [70] Chahine, J., Nymeyer, H., Leite, V. B. P., Socci, N. D., Onuchic, J. N., *Phys. Rev. Lett.* **88**, 169101 (2002).
- [71] Plaxco, K. W. *et al.*, *Nat. Struct. Biol.* **6**, 554 (1999); Ptitsyn, O. B., *Adv. Protein Chem.* **47**, 83 (1995).
- [72] Siggia, E. D., Marko, J. F., *Macromolecules* **28**, 8759 (1995).
- [73] Marenduzzo, D., Micheletti, C., *J. Mol. Biol.* **330**, 485 (2003).

[74] Tesi M. C., van Rensburg E. J. J., Orlandini E., Whittington S. G., *J. Stat. Phys.* **82**, 155 (1996).

[75] Seno, F., private communication.

[76] Cordes, M. H. J., Davidson, A. R., R. T. Sauer, *Curr. Opin. Struct. Biol.* **6**, 3 (1996).

[77] The derivation of Eq. A5 implies neglecting the chain constraint in the interaction part. It is possible but more cumbersome to take into account the chain constraint properly also here [40]. For our purposes, however it suffices to show that one obtains a term of second order in  $\rho$  in the free energy.

## APPENDIX A: MEAN FIELD CALCULATIONS

In this Appendix we derive the formulas for the mean field free energy Eqs. 13 and 14. We consider only the case of the chain of coins, the case of the polymer with triplet constraint is similar. The symbols are as in Section V A. We start from the partition function in Eq. 11:

$$\begin{aligned} \mathcal{Z} = & \int D\psi \int \prod_{i=1}^N d\vec{r}_i \int \prod_{i=1}^{N-1} d\vec{t}_i (|\vec{r}_{i+1} - \vec{r}_i| - 1) \\ & \delta(\vec{t}_i - \vec{r}_{i+1} + \vec{r}_i) \delta\left(\psi - \sum_{i=1}^N \delta(\vec{r} - \vec{r}_i) \delta(\vec{t} - \vec{t}_i)\right) \\ & e^{(-\beta \sum_{i<j;i,j=1}^N V_{2b}(\vec{r}_i - \vec{r}_j))} \prod_{i<j;i,j=1}^N (1 + f_{ij}^{(1)}) \prod_{i<j;i,j=1}^N (1 + f_{ij}^{(2)}). \end{aligned} \quad (\text{A1})$$

where, as in the text (Section V A),  $f_{ij}^{(1)}$  ( $f_{ij}^{(2)}$ ) is  $-1$  if the coins (spheres) centered in  $\vec{r}_i$  and in  $\vec{r}_j$  co-penetrate, and is  $0$  otherwise. We can rewrite Eq. A1 as:

$$\begin{aligned} \mathcal{Z} = & \int D\psi e^{-\beta \frac{1}{2} \int d\vec{r}_1 d\vec{r}_2 \psi(\vec{r}_1, \vec{t}_1) V_{2b}(\vec{r}_1 - \vec{r}_2) \psi(\vec{r}_2, \vec{t}_2)} \int \prod_{i=1}^N d\vec{r}_i \int \prod_{i=1}^{N-1} d\vec{t}_i \delta(\vec{t}_i - \vec{r}_{i+1} + \vec{r}_i) \\ & \delta(|\vec{r}_{i+1} - \vec{r}_i| - 1) \delta\left(\psi - \sum_{i=1}^N \delta(\vec{r} - \vec{r}_i) \delta(\vec{t} - \vec{t}_i)\right) \langle \mathcal{Z}_{int} \rangle(\psi). \end{aligned} \quad (\text{A2})$$

We have called:

$$\langle \mathcal{Z}_{int} \rangle(\psi) = \frac{\int_{\psi} \prod_i d\vec{r}_i d\vec{t}_i \prod_{i<j;i,j=1}^N (1 + f_{ij}^{(1)}) \prod_{i<j;i,j=1}^N (1 + f_{ij}^{(2)})}{\int_{\psi} \prod_i d\vec{r}_i d\vec{t}_i}, \quad (\text{A3})$$

where with the symbol  $\int_{\psi}$  we mean integration with respect to the density  $\psi(\vec{r}, \vec{t})$ :

$$\begin{aligned} \int_{\psi} \prod_i d\vec{r}_i d\vec{t}_i \equiv & \int \prod_i d\vec{r}_i d\vec{t}_i \delta(|\vec{r}_{i+1} - \vec{r}_i| - 1) \delta(\vec{t}_i - \vec{r}_{i+1} + \vec{r}_i) \\ & \delta\left(\psi - \sum_{i=1}^N \delta(\vec{r} - \vec{r}_i) \delta(\vec{t} - \vec{t}_i)\right). \end{aligned} \quad (\text{A4})$$

Through a standard virial or cluster expansion [68] truncated at second order in  $f^{(1)}$  and at first order in  $f^{(2)}$  [77], we get:

$$\begin{aligned} \log[\langle \mathcal{Z}_{int} \rangle(\psi)] \sim & + \frac{1}{2V} \int d\vec{r}_1 \int d\vec{r}_2 \psi(\vec{r}_1) \psi(\vec{r}_2) f^{(1)}(\vec{r}_1, \vec{r}_2) \\ & + \frac{1}{3V} \int d\vec{r}_1 \int d\vec{r}_2 \int d\vec{r}_3 \psi(\vec{r}_1) \psi(\vec{r}_2) \psi(\vec{r}_3) f^{(1)}(\vec{r}_1, \vec{r}_2) f^{(1)}(\vec{r}_2, \vec{r}_3) f^{(1)}(\vec{r}_1, \vec{r}_3) \\ & + \frac{1}{2V} \int d\vec{r}_1 \int d\vec{r}_2 \psi(\vec{r}_1) \psi(\vec{r}_2) f^{(2)}(\vec{r}_1, \vec{r}_2), \end{aligned} \quad (\text{A5})$$

where by  $\psi(\vec{r})$  we mean  $\int d\vec{t}\psi(\vec{r},\vec{t})$ . Now in Eq. A2 we use the well-known identity:

$$\delta\left(\psi - \sum_{i=1}^N \delta(\vec{r} - \vec{r}_i)\delta(\vec{t} - \vec{t}_i)\right) = \int D\hat{\psi} e^i \int d\vec{r} \int d\vec{t} \hat{\psi}(\vec{r},\vec{t}) \psi(\vec{r},\vec{t}) - \sum_{i=1}^N \hat{\psi}(\vec{r}_i,\vec{t}_i). \quad (\text{A6})$$

In this way we can rewrite eq. A2 as in Eq. 13 with:

$$\begin{aligned} \mathcal{H}(\psi, \hat{\psi}) = & +\frac{1}{2} \int d\vec{r}_1 d\vec{r}_2 \psi(\vec{r}_1, \vec{t}_1) V_{2b}(\vec{r}_1 - \vec{r}_2) \psi(\vec{r}_2, \vec{t}) - i \int d\vec{r} d\vec{t} \hat{\psi}(\vec{r}, \vec{t}) \psi(\vec{r}, \vec{t}) \\ & - \log(\zeta(\hat{\psi})) - \frac{1}{2V} \int d\vec{r}_1 \int d\vec{r}_2 \psi(\vec{r}_1) \psi(\vec{r}_2) f^{(1)}(\vec{r}_1, \vec{r}_2) \\ & - \frac{1}{3V} \int d\vec{r}_1 \int d\vec{r}_2 \int d\vec{r}_3 \psi(\vec{r}_1) \psi(\vec{r}_2) \psi(\vec{r}_3) f^{(1)}(\vec{r}_1, \vec{r}_2) f^{(1)}(\vec{r}_2, \vec{r}_3) f^{(1)}(\vec{r}_1, \vec{r}_3) \\ & - \frac{1}{2V} \int d\vec{r}_1 \int d\vec{r}_2 \psi(\vec{r}_1, \vec{t}_1) \psi(\vec{r}_2, \vec{t}_2) f^{(2)}(\vec{r}_1, \vec{r}_2) \end{aligned} \quad (\text{A7})$$

where we have called  $\zeta(\hat{\psi})$  the polymeric partition function, which reads:

$$\zeta(\hat{\psi}) \equiv \left( \int \prod_i d\vec{r}_i \delta(|\vec{r}_{i+1} - \vec{r}_i| - 1) e^{-i \sum_{i=1}^N \hat{\psi}(\vec{r}_i, \vec{t}_i)} \right)^{\frac{1}{N}}. \quad (\text{A8})$$

The saddle point equations read  $\frac{\delta\mathcal{H}}{\delta\psi} = \frac{\delta\mathcal{H}}{\delta\hat{\psi}} = 0$ . Solving this equation instead of finding the full partition function is effectively a mean field approximation (the path we follow is reminiscent of that used in Ref. [66]). In this form this equation is still not solvable explicitly. As in the text, we make the further approximation  $\psi(\vec{r}, \vec{t}) \equiv \rho\phi(\vec{t}) \equiv \psi(\vec{t})$  (and consequently from the saddle point equations one finds  $\hat{\psi}(\vec{r}, \vec{t}) \equiv \hat{\rho}\hat{\phi}(\vec{t}) \equiv \hat{\psi}(\vec{t})$ ). One obtains  $\zeta(\hat{\psi}) = \int d\vec{t} \delta(|\vec{t}| - 1) e^{-i\hat{\psi}(\vec{t})}$  and the equation  $\frac{\delta\mathcal{H}}{\delta\psi} = 0$  takes on the form of a self-consistent equation for  $\psi$  and  $\hat{\psi}$ :

$$\psi(\vec{r}, \vec{t}) = \rho \frac{e^{-i\hat{\psi}(\vec{t})}}{\int d\vec{t} \delta(|\vec{t}| - 1) e^{-i\hat{\psi}(\vec{t})}} \quad (\text{A9})$$

or equivalently:

$$-i\hat{\psi}(\vec{t}) = \log\left(\frac{\langle e^{-i\hat{\psi}(\vec{t})} \rangle \psi(\vec{r}, \vec{t})}{\rho}\right) \quad (\text{A10})$$

where with  $\langle \cdot \rangle$  we denote ensemble averaging with respect to the measure  $\int d\vec{t} \delta(|\vec{t}| - 1) \cdot$ . To we recover the free energy in Eqs. 14, we need to recall also the formula for the mean excluded volume of two coins, with axis  $\vec{t}_1$  and  $\vec{t}_2$ , and radius  $R_0$  which is due to Onsager [67] and reads:

$$\frac{1}{2V} \int d\vec{r}_1 \int d\vec{r}_2 f^{(2)}(\vec{r}_1, \vec{r}_2; \vec{t}_1, \vec{t}_2) = -2\pi R_0^3 \left(1 - (\vec{t}_1 \cdot \vec{t}_2)^2\right)^{\frac{1}{2}}. \quad (\text{A11})$$

Inserting Eqs. A8 into Eq. 13, and using Eq. A10, we obtain Eq. 14.

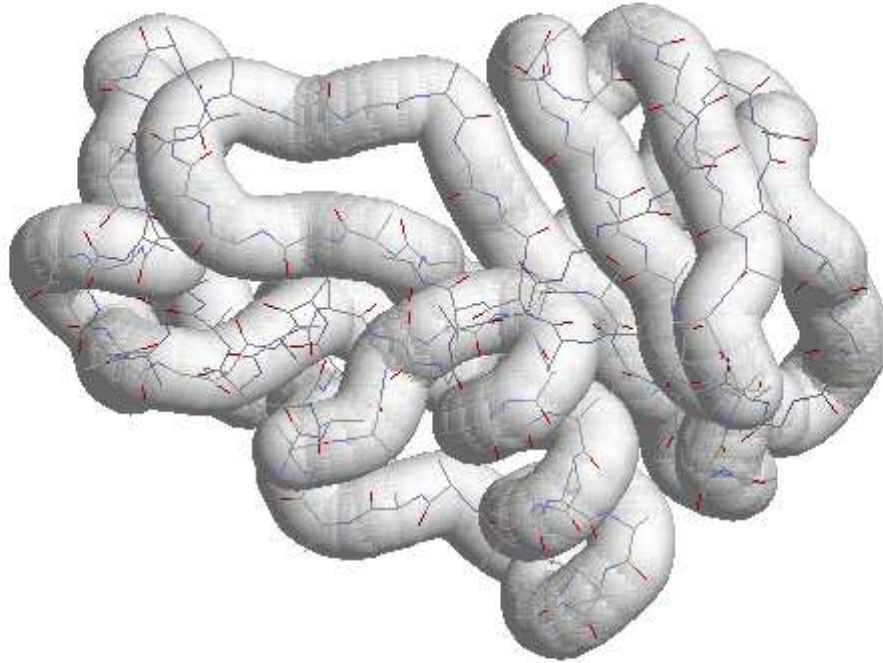


FIG. 1. An all atom representation of a segment of protein backbone (thin colored lines) together with its corresponding backbone 'tube'. The backbone  $C_\alpha$  atoms and the side chains of the amino acids impose steric constraints which leads to an effective tube of non-zero thickness. The tube is not inflated up to its maximum thickness for convenience of visualization.

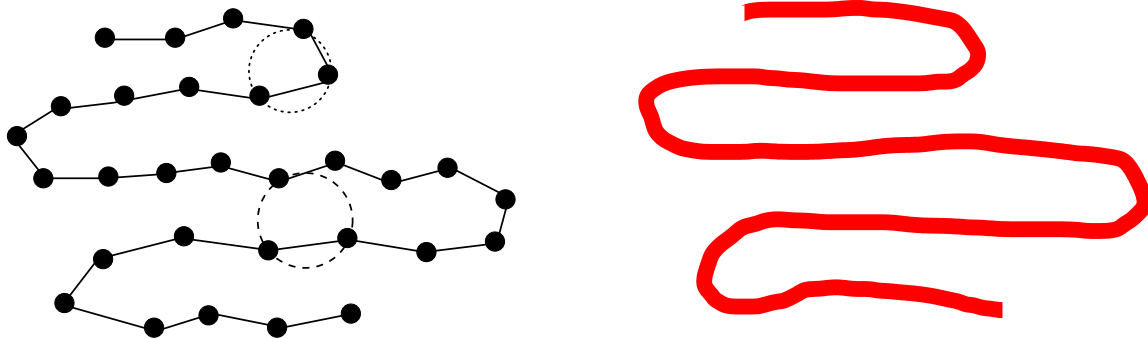


FIG. 2. Left: sketch of the backbone of a chain representing a discrete thick polymer: the black spheres are the position of monomers, the thickness is imposed by requiring that no triplet radii is bigger than the required thickness  $R_0$ : two such radii, one involving consecutive points (dotted line) and one non-consecutive points (dashed line) are shown. Right: the continuum counterpart of the discrete polymer is the red tube drawn here.

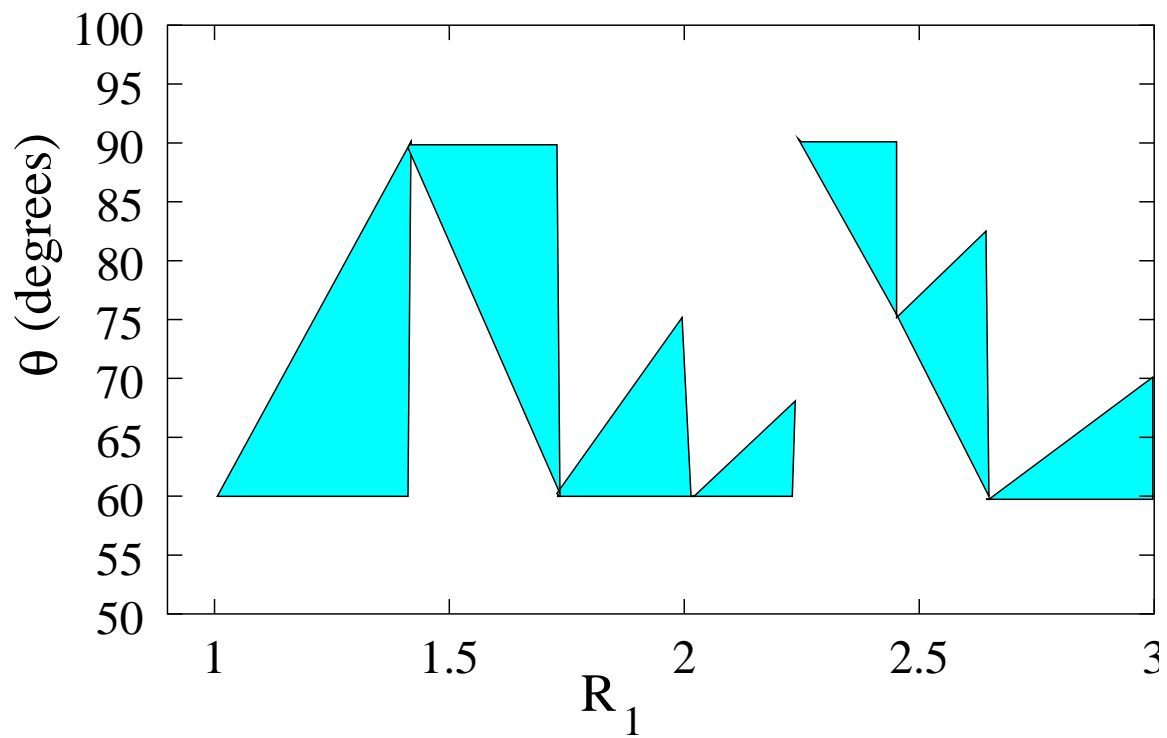


FIG. 3. Sketch of the structural symmetry of a chain of hard disks in two dimensions as a function of the range of the attraction (measured in units of the disk diameter). The angle  $\theta$  denotes the symmetry of the lattice. For example  $60^\circ$  refers to a triangular lattice and  $90^\circ$  to a square lattice. The shaded region shows that the ground state is degenerate with all angles in the shaded region forming the ground state spectrum.

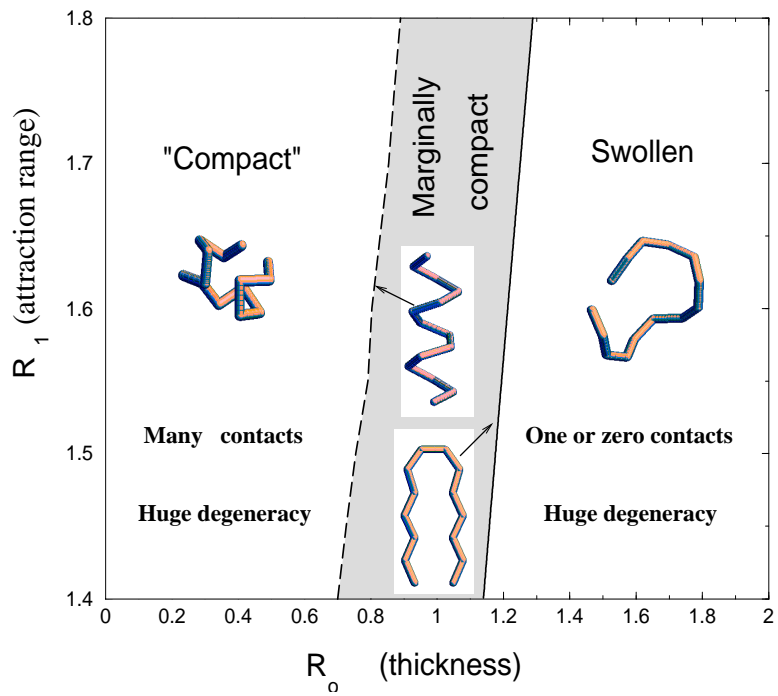


FIG. 4. Sketch of phases, their characteristics and the associated ground state structures of short tubes in the  $R_0$ - $R_1$  plane at low temperatures.



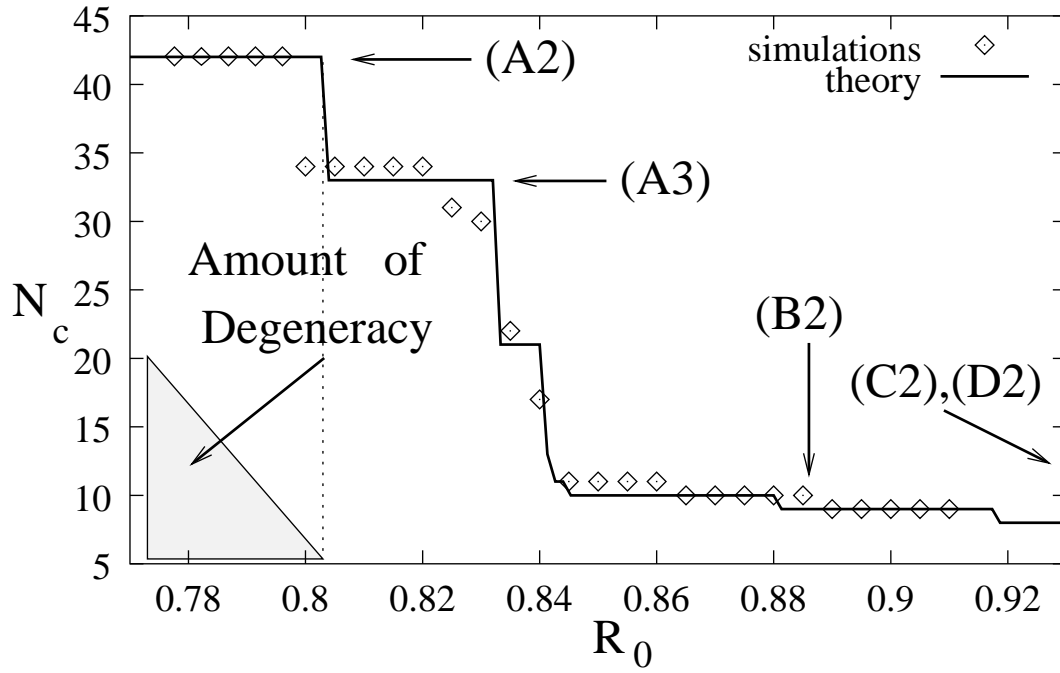


FIG. 5. Plot of the number of contacts,  $N_c$ , vs.  $R_0$  for a short thick tube ( $N = 14$ ). The labels (A2), (A3), (B2), (C2) and (D2) refer to unique ground state structures shown in Figure 6. The points show the results obtained in the simulations, whereas the line was obtained by means of analytic calculations carried out for idealized structures. The triangle at the left corner depicts qualitatively the degree of degeneracy of the ground state structures. For example, the degeneracy at 0.78 is proportional to the height of the triangle at that point and the degeneracy at 0.80 is 1.

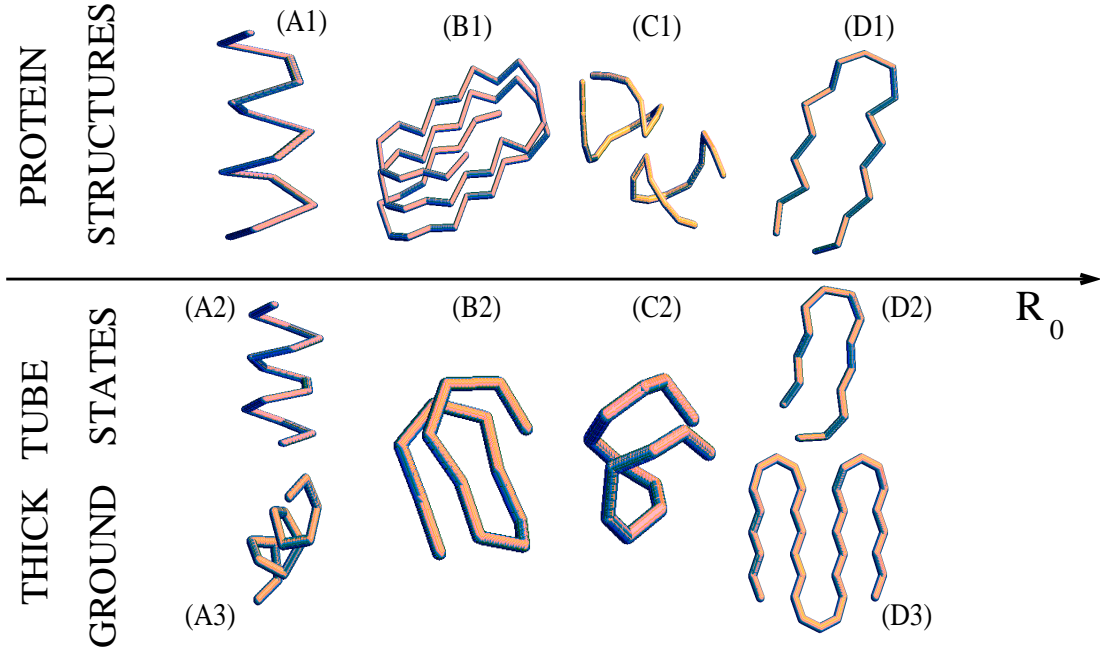


FIG. 6. Building blocks of biomolecules and ground state structures associated with the marginally compact phase of a short tube. The axis in the middle indicates the direction along which the tube thickness  $R_0$  increases. The top row shows some of the building blocks of biomolecules, while the bottom row depicts the corresponding structures obtained as the ground state conformations of a short tube. (A1) is an  $\alpha$ -helix of a naturally occurring protein, while (A2) and (A3) are the helices obtained in our calculations – (A2) has a regular contact map and is obtained when  $R_0 = 0.80$  whereas (A3) ( $R_0 = 0.83$ ) is a distorted helix in which the distance between successive atoms along the helical axis is not constant but has period 2. (B1) is a helix of strands in the alkaline protease of *pseudomonas aeruginosa*, whereas (B2) shows the corresponding structure ( $R_0 = 0.88$ ) obtained in our computer simulations. (C1) shows the “kissing” hairpins of RNA and (C2) the corresponding conformation obtained in our simulations with  $R_0 = 0.95$ . Finally (D1) and (D2) are two instances of quasi-planar hairpins. The first structure is from the same protein as before (the alkaline protease of *pseudomonas aeruginosa*) while the second is a typical conformation found in our simulations when  $R_0 > 0.98$ . All the cases shown correspond to tubes of 14 spheres, except for the sheet-like structure (D3), which employed 33 spheres. This figure also appeared in Ref. [20].

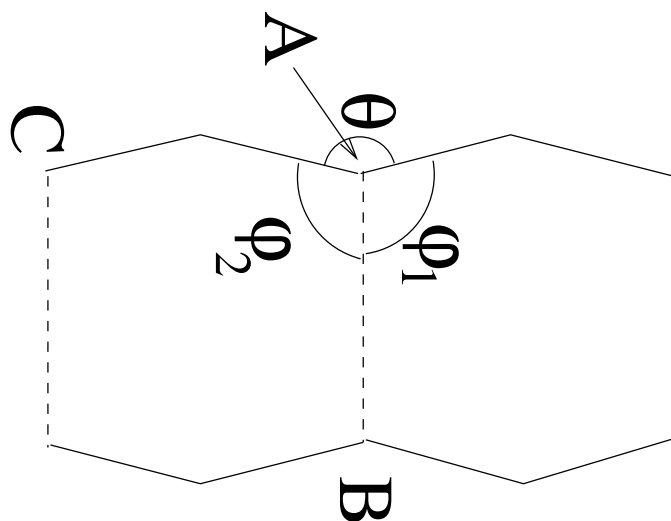


FIG. 7. A schematic view of portions of two zig-zag strands facing each other. The angles  $\theta$ ,  $\phi_{1,2}$ , and the points A, B, C which are referred to in the text are shown.

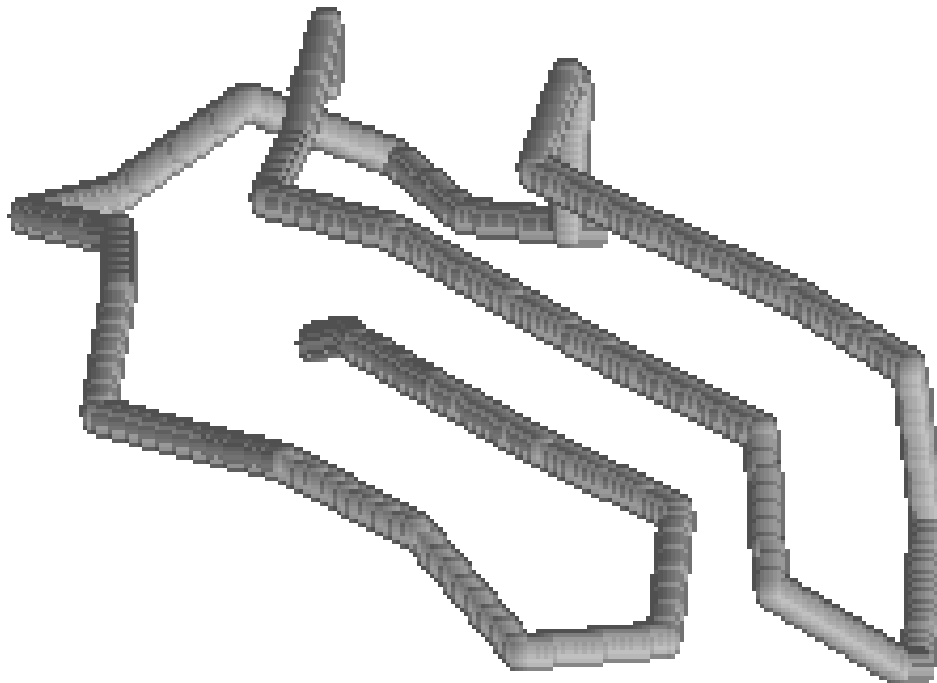
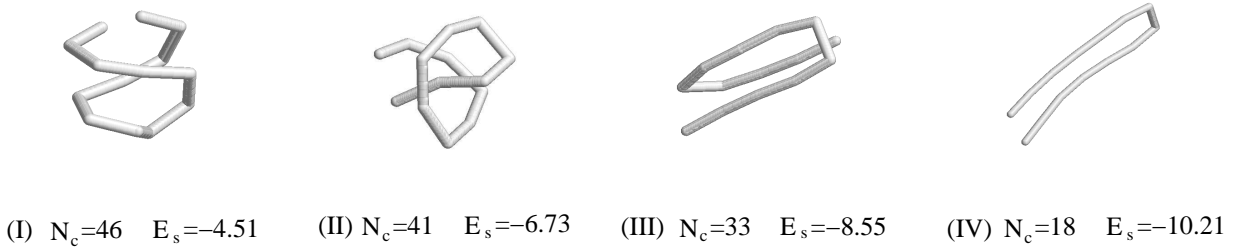
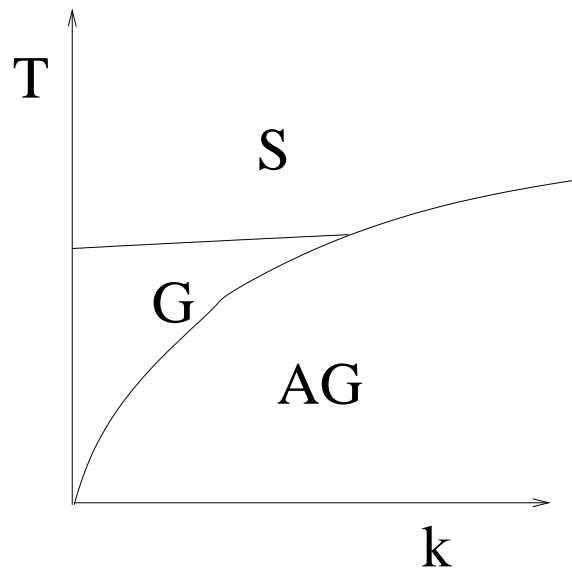


FIG. 8. One of the low energy states for a tube of thickness 0.9 with 41 beads. Note the parallel alignment of neighbouring tube segments.



$N=14$   $N_c=46$   $E_s=-2.55$      $N=14$   $N_c=44$   $E_s=-4.42$      $N=22$   $N_c=83$   $E_s=-9.63$      $N=22$   $N_c=80$   $E_s=-10.36$

FIG. 9. In this figure we show the ground states obtained for a semiflexible chain of increasing stiffness. The notes under each configurations indicate its number of contacts and the value of the stiffness term  $E_s$  (see the text for its definition). The labels I, II, III and IV are discussed in the text. Conformations in the first row have chain length  $N = 14$ .



stiff polymer

FIG. 10. Schematic phase diagram of a stiff polymer. The phases are  $S$ =Swollen,  $G$ =globule, and  $AG$ = Asymmetric globule.

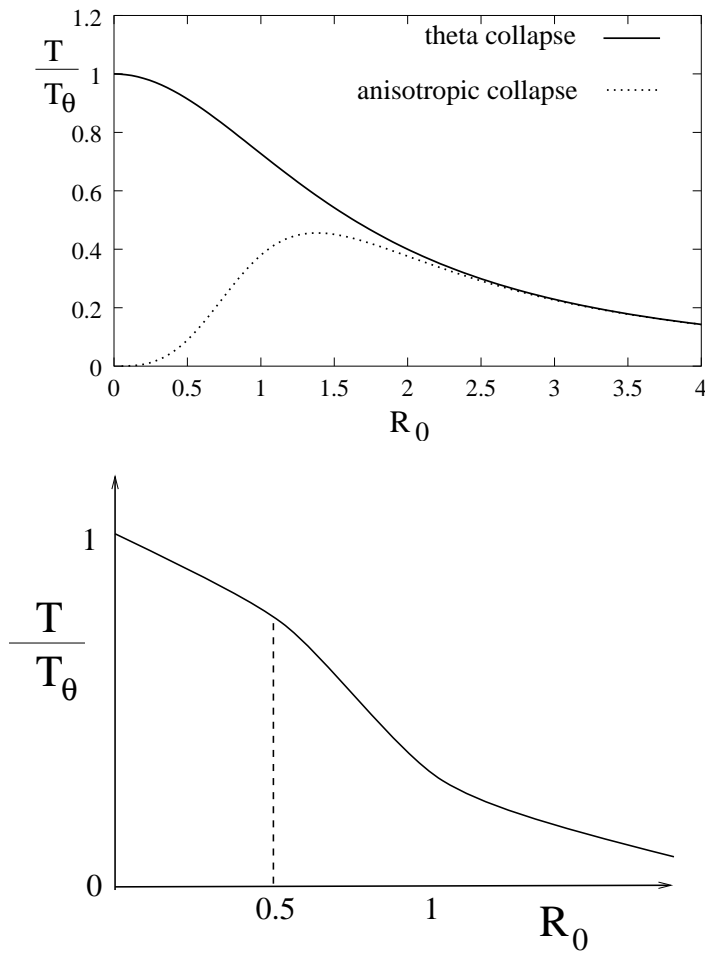


FIG. 11. Schematic phase diagrams of a chain of coins (top panel) and of a tube with a three body constraint (bottom panel) in the  $(T, R_0)$  plane obtained in the mean field approximation.

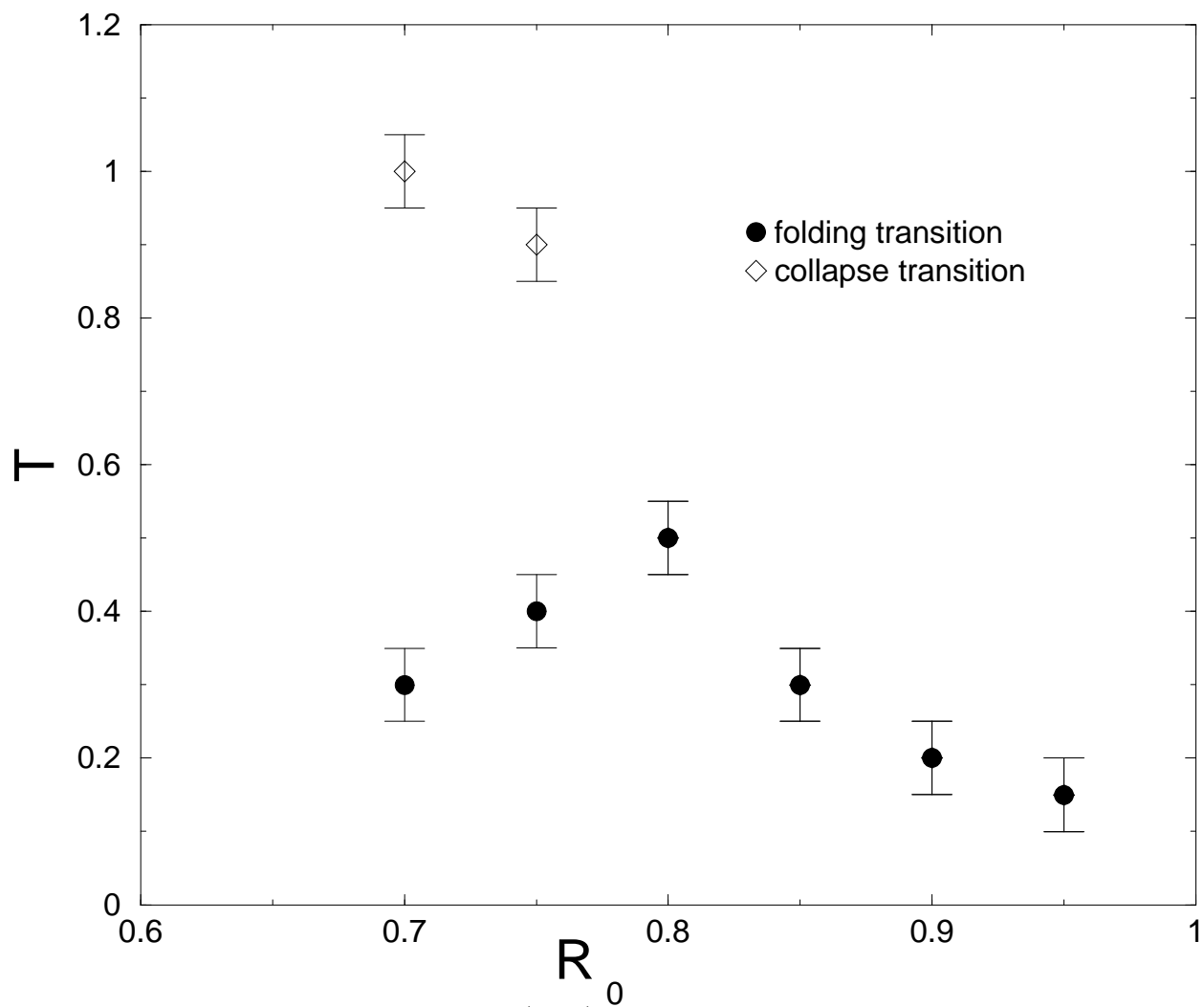
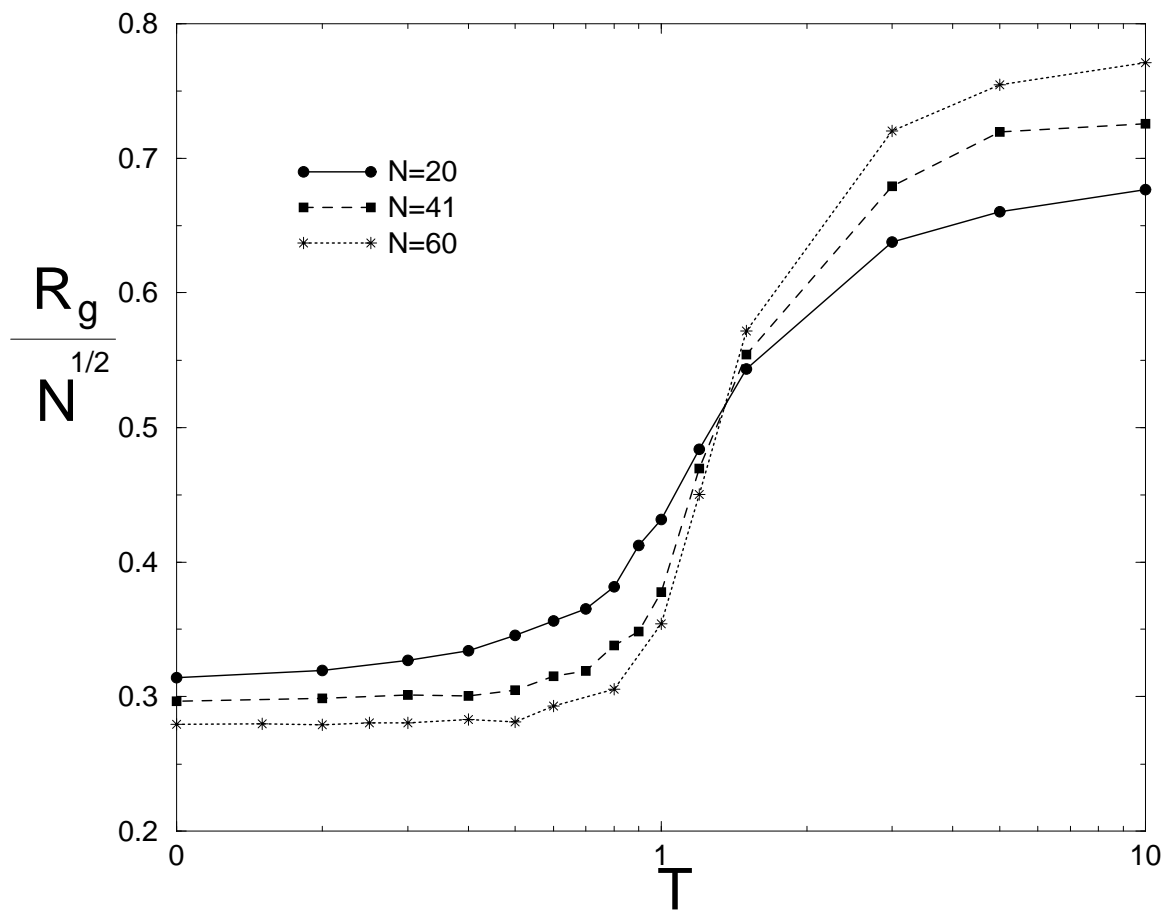


FIG. 12. Phase diagram for a thick polymer in the  $(T, R_0)$  plane obtained with Monte-Carlo simulations. The points represent peaks in the specific heat curve for  $N = 41$ .





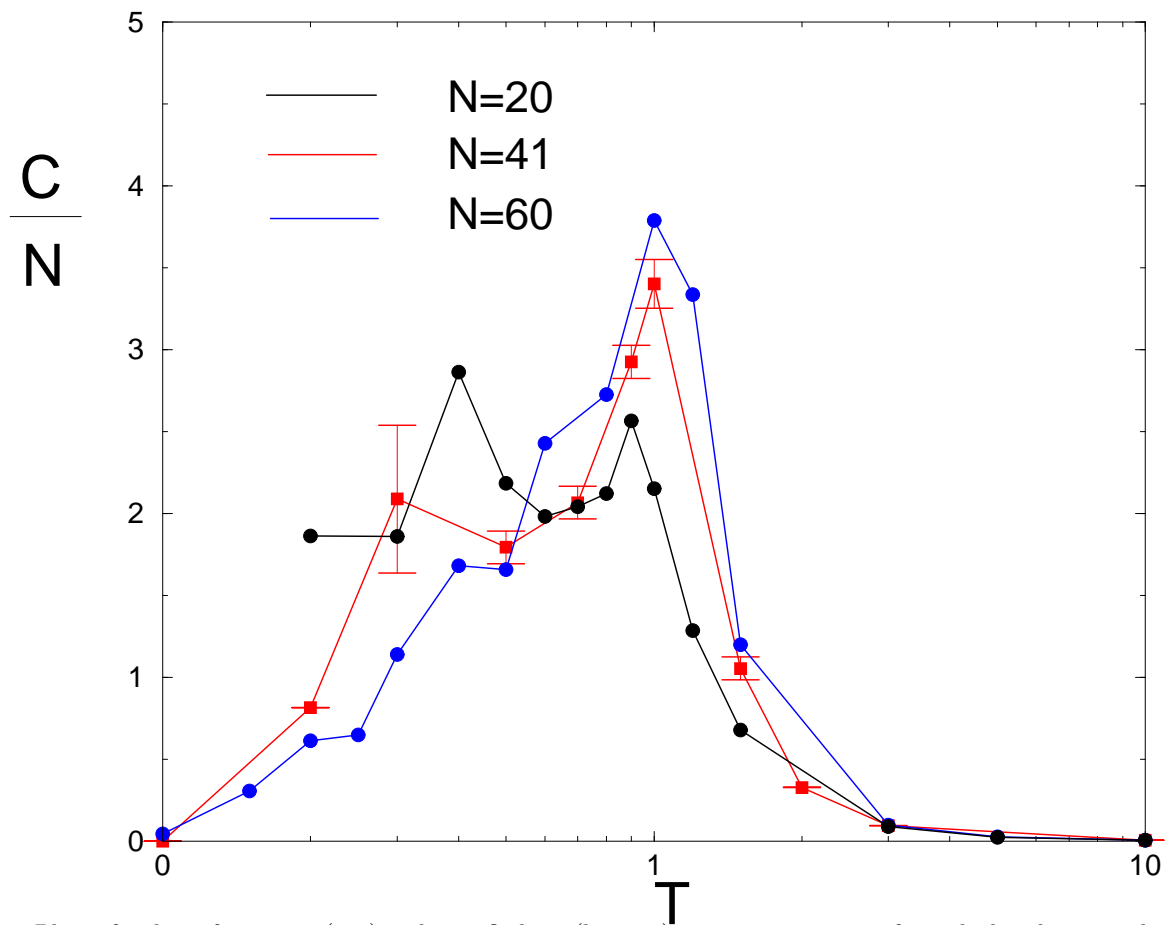
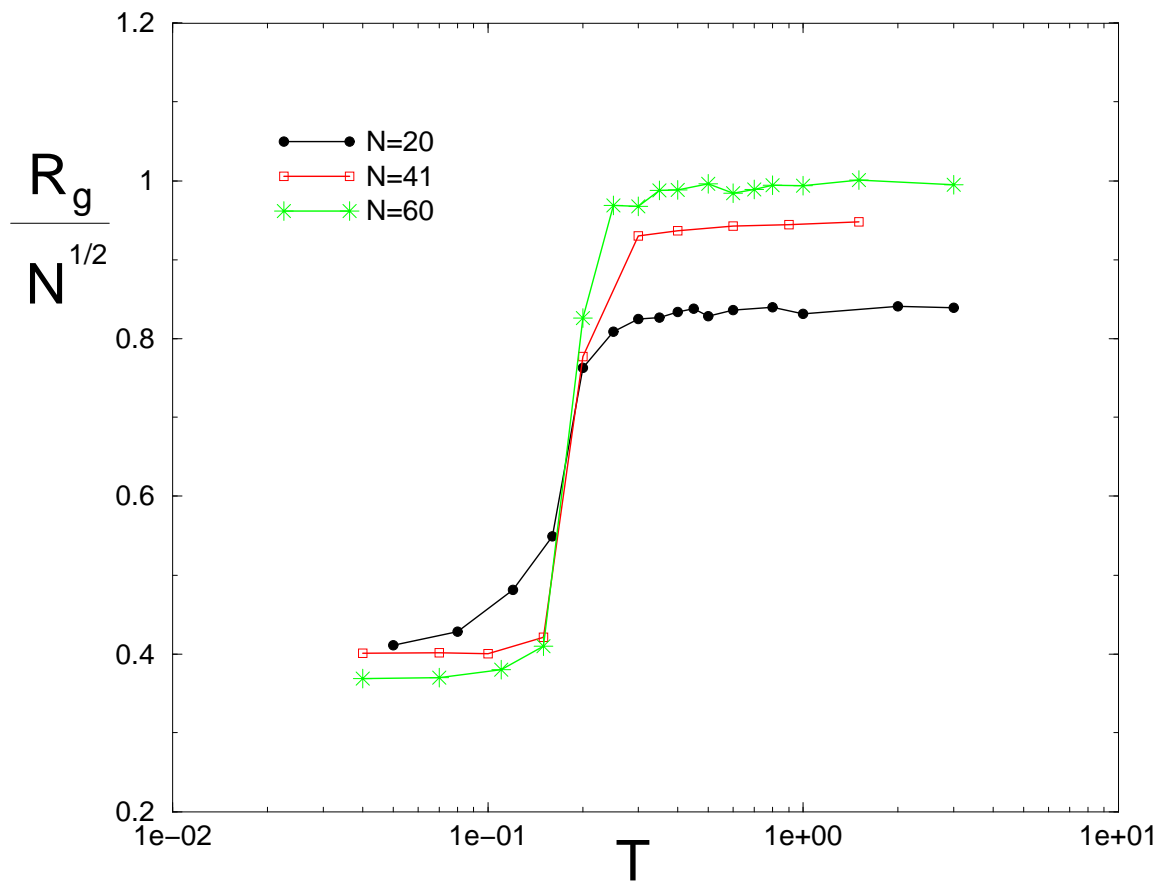


FIG. 13. Plots of radius of gyration (top) and specific heat (bottom) versus temperature for a thick polymer with  $R_0 = 0.7$ . The error bars in the radius of gyration estimate are comparable to the point size. For clarity, we have shown error bars in the specific heat only for  $N = 41$ , for which we have carried out the most extensive simulations.



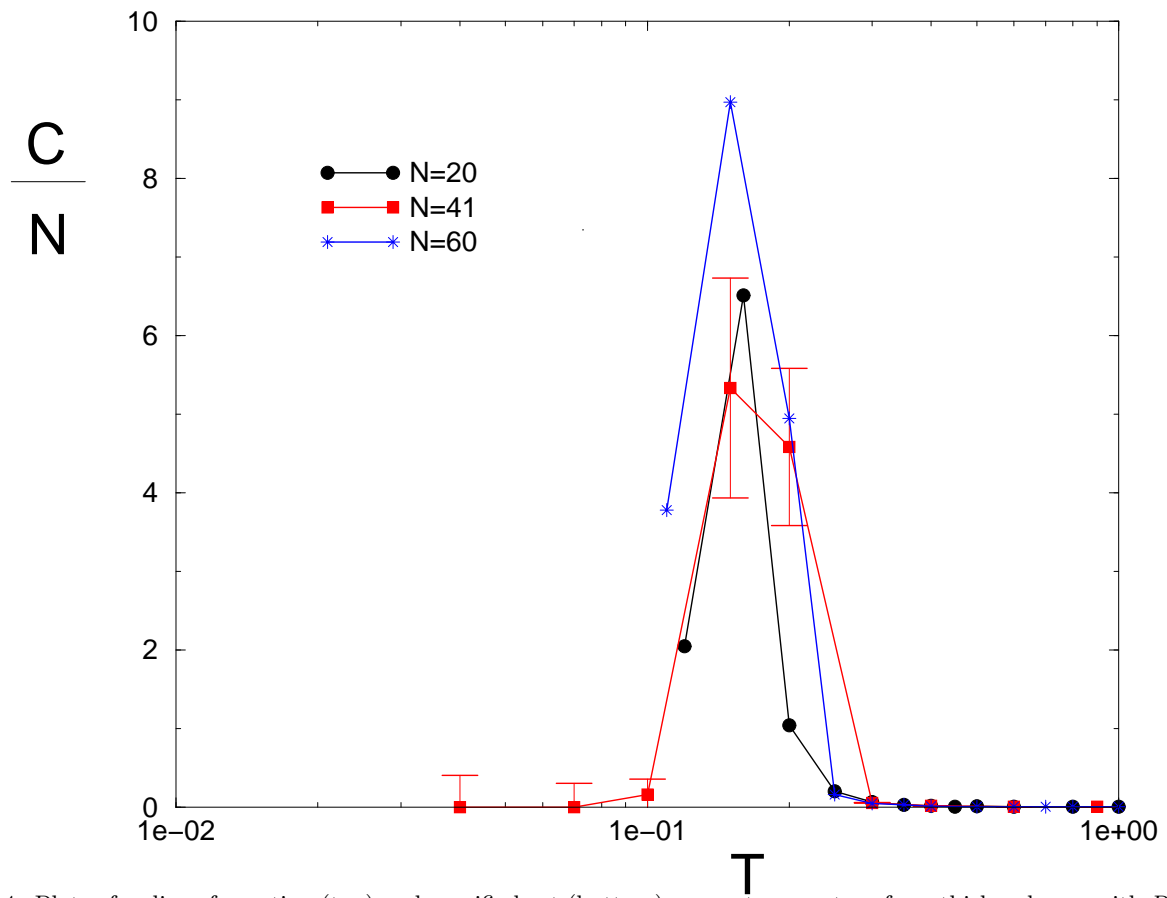


FIG. 14. Plots of radius of gyration (top) and specific heat (bottom) versus temperature for a thick polymer with  $R_0 = 0.95$ . The error estimates are as described in the caption of Fig. 13

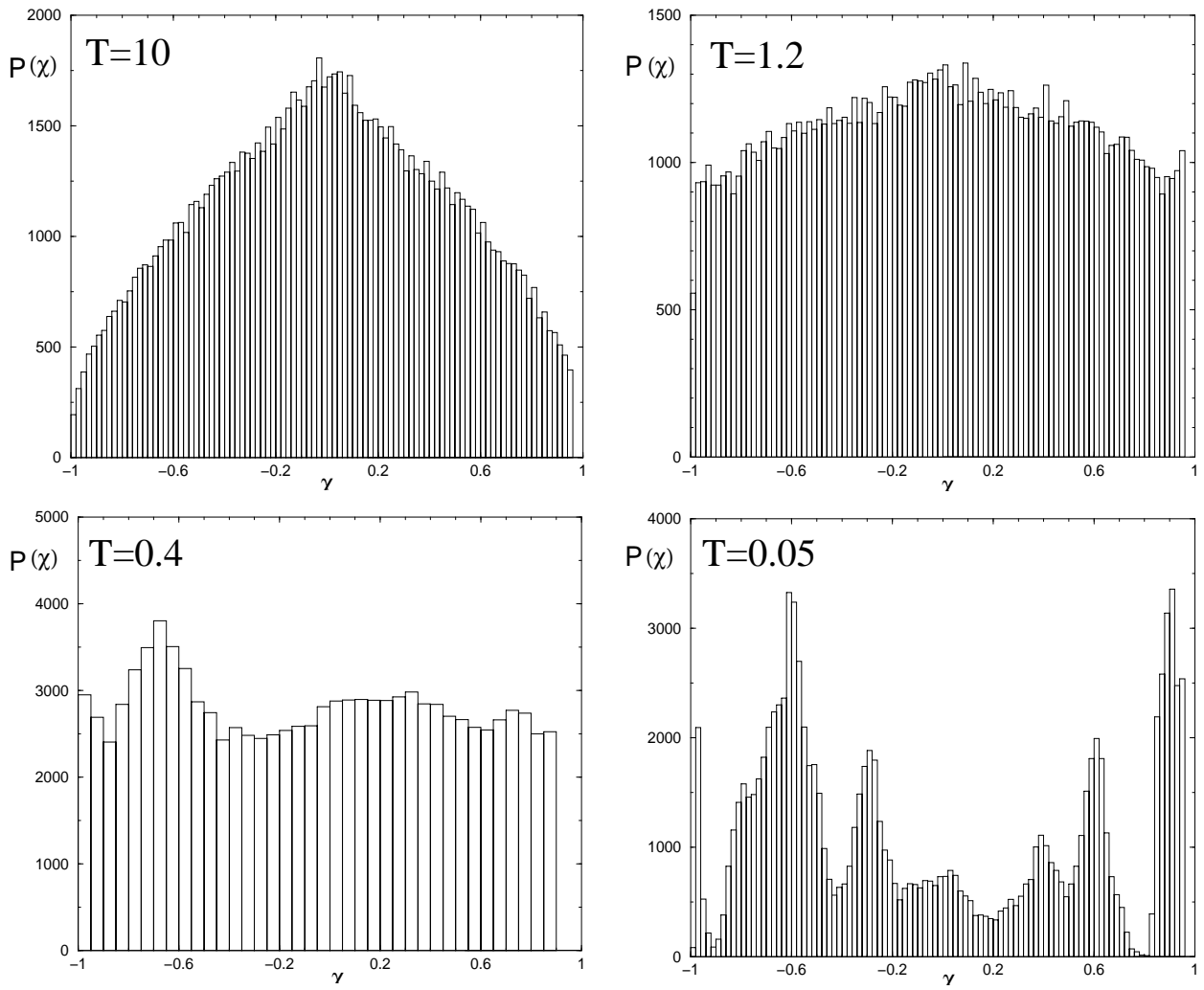


FIG. 15. Chirality probability distribution (unnormalized) from Monte-Carlo simulations for a thick polymer with  $R_0 = 0.7$ .

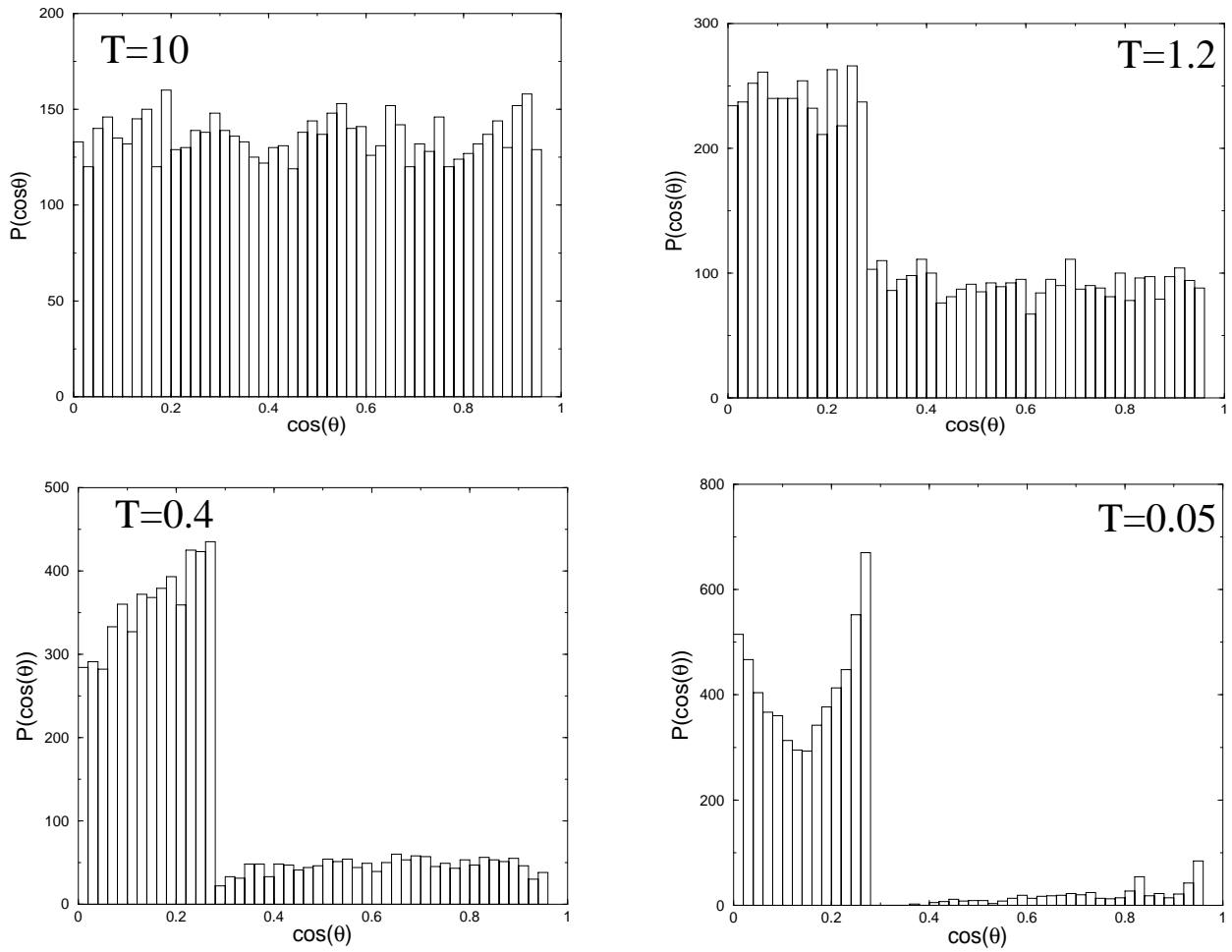


FIG. 16. Unnormalized probability distribution of  $\cos(\theta)$  for  $R_0 = 0.7$ . The  $x$ -axis scale begins at 0 because  $R_0 = 0.7$  yields a constraint on the local thickness that  $\cos\theta$  must be greater than  $-0.02\dots$  and virtually no points have negative  $\cos\theta$ .

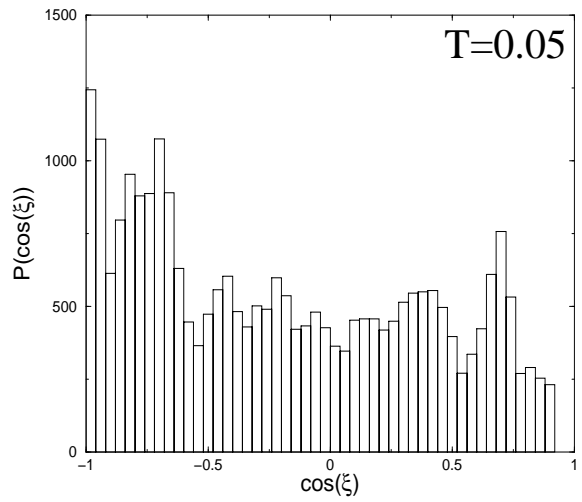
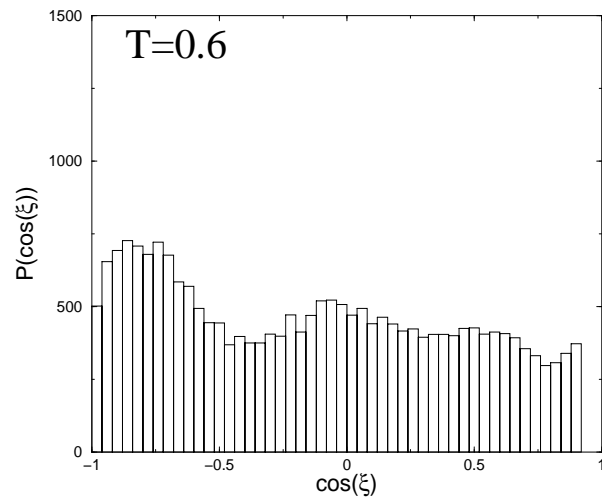
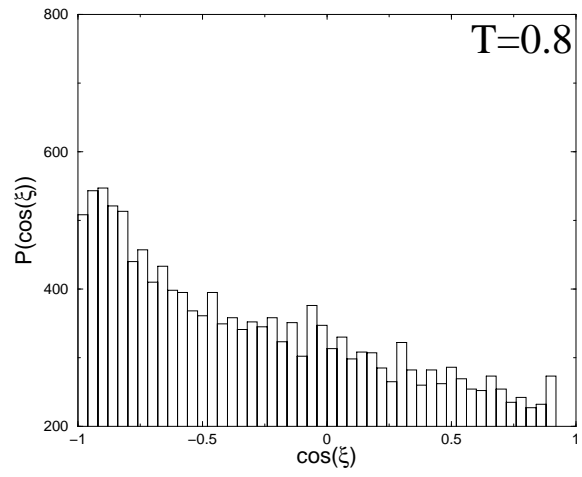
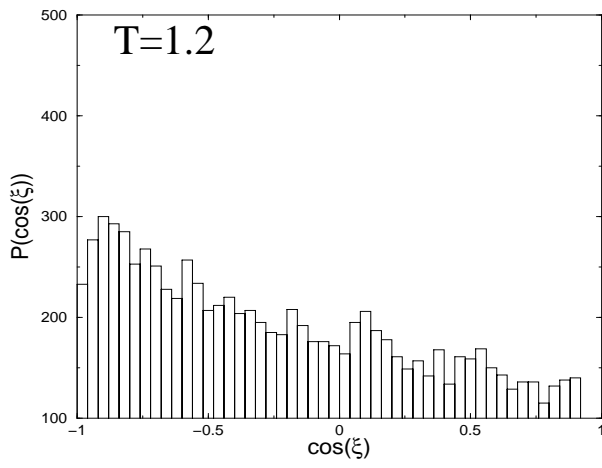


FIG. 17. Unnormalized probability distribution of  $\cos(\xi)$  for  $R_0 = 0.7$ .

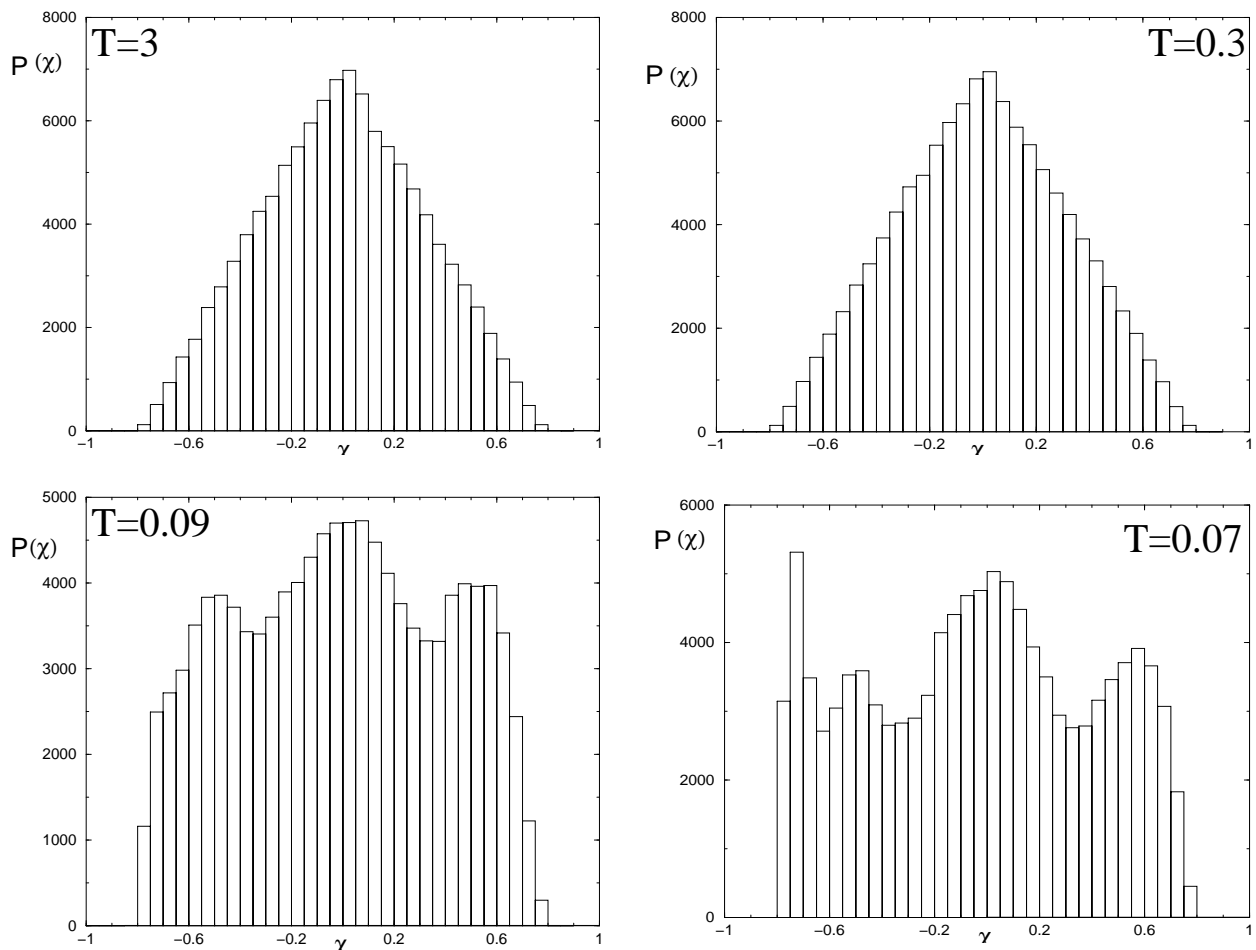


FIG. 18. Chirality probability distribution (unnormalized) from Monte-Carlo simulations for a thick polymer with  $R_0 = 0.95$ .

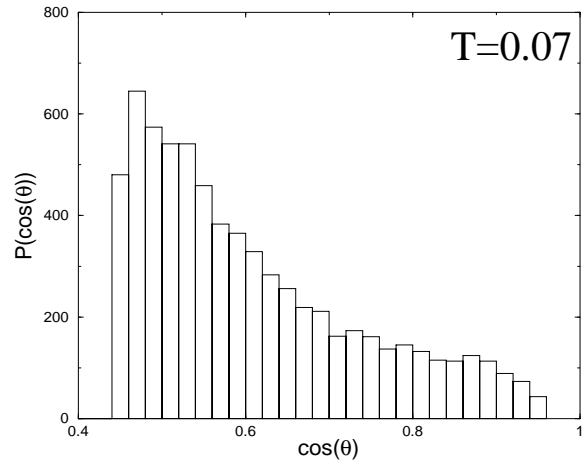
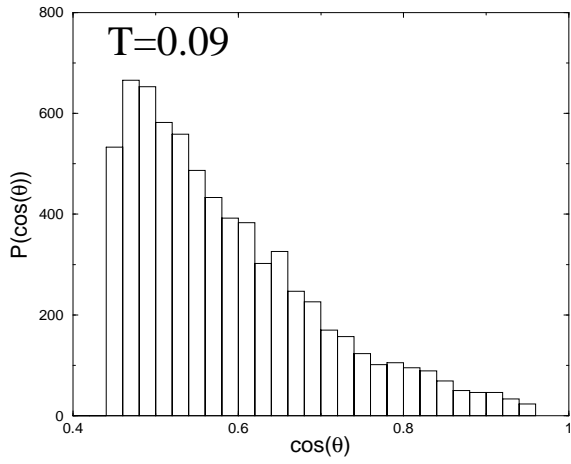
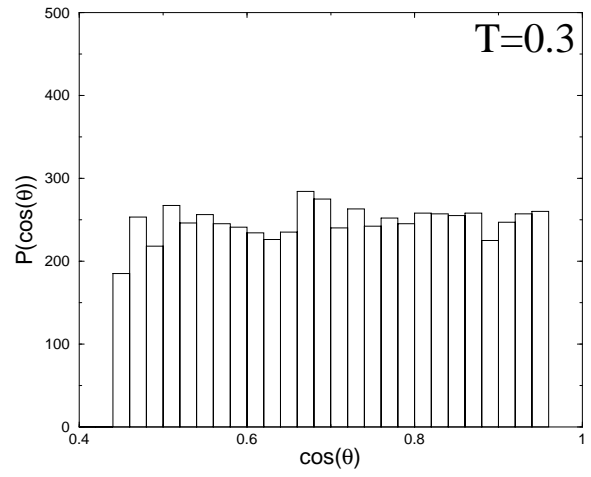
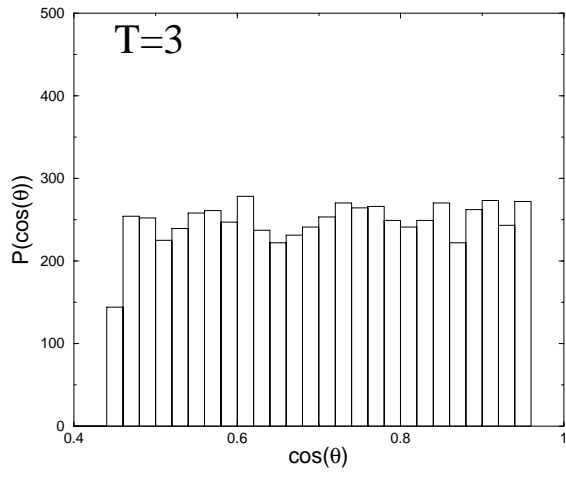


FIG. 19. Unnormalized probability distribution of  $\cos(\theta)$  for  $R_0 = 0.95$ .



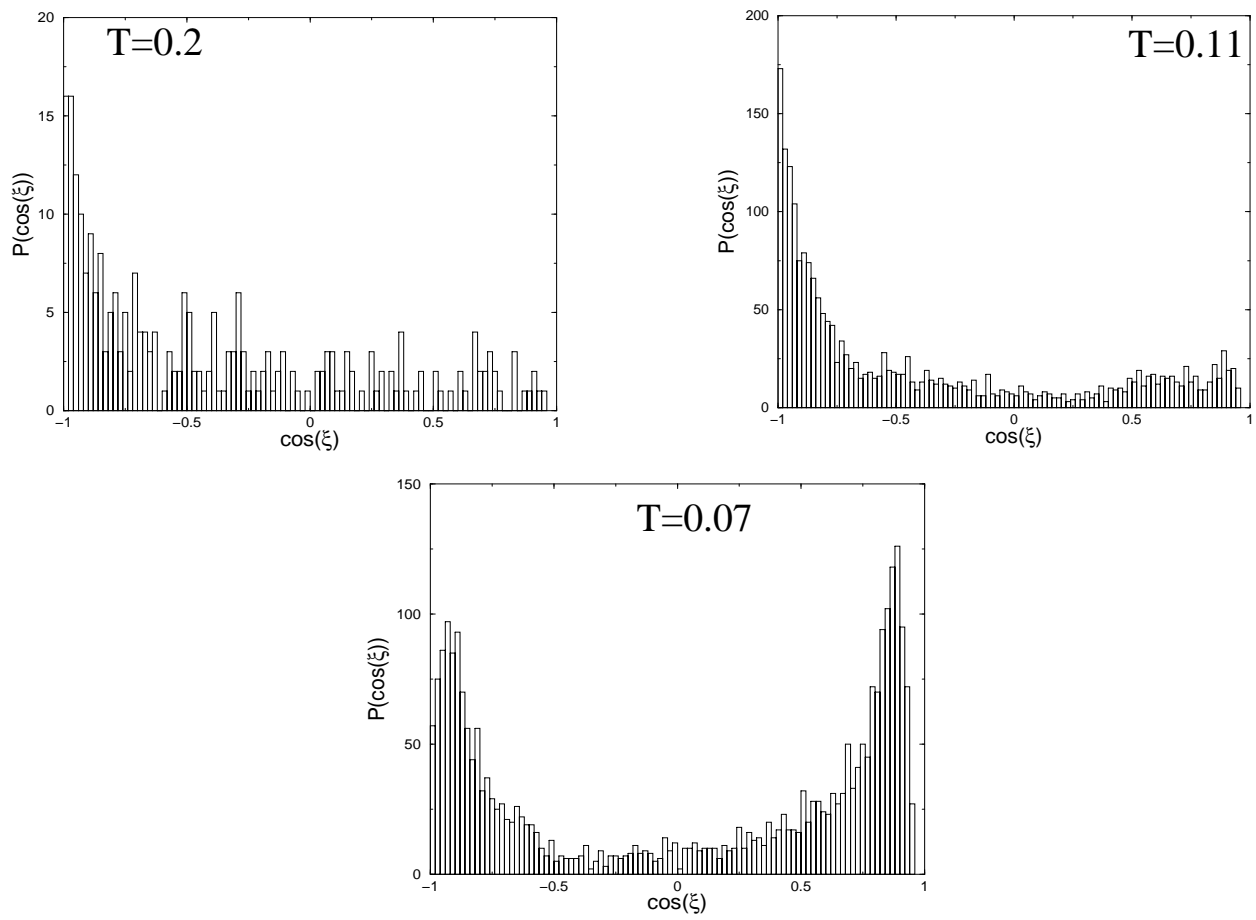


FIG. 20. Unnormalized probability distribution of  $\cos(\xi)$  for  $R_0 = 0.95$ .